Loss of accumulation zone exposes dark ice and drives increased ablation at Weißseespitze, Austria

Lea Hartl[1, 2], Federico Covi[3], Martin Stocker-Waldhuber[1], Anna Baldo[1, 4], Davide Fugazza[4], Biagio Di Mauro[5], and Kathrin Naegeli[6]

[1]Institute for Interdisciplinary Mountain Research, Austrian Academy of Sciences, Innrain 25, 6020 Innsbruck, Austria
[2]Alaska Climate Research Center, University of Alaska Fairbanks, 2156 Koyukuk Drive, Fairbanks, AK 99775, USA
[3]British Antarctic Survey, Cambridge, United Kingdom
[4]Consiglio Nazionale delle Ricerche - Istituto di Scienze Polari, Milan, Italy
[5]Department of Environmental Science and Policy, Università degli Studi di Milano, Milan, Italy
[6]Department of Geography, University of Zurich, Zurich, Switzerland

Correspondence: L. Hartl (lea.hartl@oeaw.ac.at)

Abstract. In recent years, firn and summer snow cover has decreased on Alpine glaciers, exposing larger areas of ice at higher elevations. This reduces albedo and leads to increased melt. To understand mass loss in former accumulation areas under conditions of rapid glacier recession, it is important to constrain the possible range of ice albedo in newly firn free regions, the duration of ice exposure, and the albedo-ablation connection. We combine data from an on-ice weather station (3492 m.a.s.l.),
5 ablation stakes, and remote sensing derived albedo to provide an overview of albedo and ablation in the summit region of Weißseespitze, the high-point of Gepatschferner (Austria), from 2018 to 2024. Before 2022, low albedo (<0.4) occurred on 3 to 8 days per year. In 2022, 37 days of low albedo conditions were recorded and albedo dropped below previously observed minima of around 0.30 to values similar to those of the surrounding rock. Albedo remained very low in 2023 and 2024. Ice ablation at the stakes generally increased with the duration of ice exposure, reaching up to -1.6 m w.e. in high-melt years.
10 Sensitivity experiments indicate that a five day period of very low albedo conditions (<0.20) results in 31% more modeled surface melt if it occurs in late July compared to early September, highlighting temporal variability in the impact of ice exposure. The unique Weißseespitze dataset provides a starting point for further studies linking causes and effects of albedo changes in former accumulation zones.

15 # 1 Introduction

Glaciers outside the polar regions are losing mass at unprecedented rates (Hugonnet et al., 2021; Jakob and Gourmelen, 2023), with projected mass losses of up to 41% by 2100 globally (Rounce et al., 2023) and up to 94% in the Alps (Zekollari et al., 2019), where complete glacier loss is anticipated regionally in the coming decades (Hartl et al., 2024a).

During recent extreme melt seasons, repeated heat waves contributed to extreme glacier mass loss in the Alps (Cremona et al., 2023; Voordendag et al., 2023) and glacier thinning was observed in the highest reaches of Alpine glaciers (Berthier et al., 2023; Hartl et al., 2024b). As snow lines rise and multi-year firn is depleted, darker, bare ice becomes exposed. This albedo decrease affects surface energy balance by increasing the amount of solar radiation absorbed by the ice surface, leading to a positive melt-albedo feedback. Albedo correlates strongly with glacier mass balance in the Alps and other mountain regions, highlighting the importance of this feedback for glacier evolution (e.g. Dumont et al., 2012; Zhang et al., 2021; Di Mauro and Fugazza, 2022).

As global glacier recession accelerates (Hugonnet et al., 2021), ice albedo, its variability in time and space, and drivers thereof have increasingly come into focus. At local and regional scales, ice albedo depends on meteorological (solar elevation, cloudiness, radiation budget; Volery et al., 2025) and topographic (surface roughness; Irvine-Fynn et al., 2014) factors, on the ice properties (liquid water, pore space characteristics; Dadic et al., 2013), weathering crust onset (Traversa and Di Mauro, 2024), and on the presence of light absorbing impurities of organic and inorganic origin, including black carbon, algae, and dust (Oerlemans et al., 2009; Di Mauro et al., 2017; Goelles and Bøggild, 2017).

Spaceborne remote sensing observations have been used to assess regional trends and seasonality of glacier albedo (Naegeli et al., 2019; Fugazza et al., 2019; Gunnarsson et al., 2021; Marshall, 2021; Shaw et al., 2021; Williamson and Menounos, 2021; Di Mauro and Fugazza, 2022; Traversa and Di Mauro, 2024). Some of the driving processes of albedo variability can be detected in remote sensing data, for example changes in debris cover (e.g. Azzoni et al., 2016), deposition of light absorbing particles related to dust or volcanic eruptions (Di Mauro et al., 2017; Gunnarsson et al., 2023), and the presence of algae (Di Mauro et al., 2020). Several studies have shown a negative trend in ice albedo, or "glacier darkening", in the Alps (Naegeli et al., 2019; Fugazza et al., 2019; Di Mauro and Fugazza, 2022); however, the magnitude of trends differs between regions.

Satellite derived albedo products have been used to drive glacier energy balance models (e.g. Gunnarsson et al., 2023), but typically do not fully resolve small scale albedo variability (e.g. Hartl et al., 2020; Rossini et al., 2023). Remote sensing time series are often discontinuous due to limitations related to cloud cover and frequency of satellite overpasses. Large scale reanalysis products and modeled albedo can show large discrepancies with observed albedo over glacier surfaces (e.g. Draeger et al., 2024).

Accordingly, in situ data are key as ground truth for remote sensing products and can complement sparse remote sensing time series as well as contribute to calibration and validation exercises (Di Mauro et al., 2024). Continuous in situ albedo measurements on glacier surfaces remain rare (Ren et al., 2021) and long-term monitoring sites are essential for assessing the potential range of bare ice albedo and how this may change over time. Such information is also needed to improve albedo parametrization schemes in energy balance modeling, which often struggle to reproduce the observed spatial and temporal variability of glacier albedo (e.g. Brock et al., 2000, 2006; Collier et al., 2013; Eidhammer et al., 2021).

The continued loss of firn and reduced seasonal snow cover during extreme years increases the relative importance of bare ice and the potential albedo variability of bare ice surfaces for glacier-wide albedo. In addition to impacts on glacier-wide mass balance, the exposure of bare ice at high elevations has important implications for mass balance gradients, which play a key role in large-scale glacier modeling and future projections (e.g. Miles et al., 2021; Schuster et al., 2023). Paul et al. (2005)

described the impact of reduced summer snow cover on albedo and mass loss during the exceptionally warm summer of 2003

55 in Switzerland. They noted that loss of snow cover at high elevations can lead to an inverted mass balance profile, pointing out
the need for assimilation of albedo observations in mass balance modeling.

In the following, we explore a unique, multi-scale dataset of in situ meteorological observations, remote sensing derived
albedo, and a network of ablation stakes from the highest region of Gepatschferner, Austria's second-largest glacier. We provide
a quantitative overview of bare ice albedo in the summit region and (former) accumulation zone for recent years (2018-2024).

60 We focus on snow free periods and interannual albedo variability in context with ablation measurements and the sensitivity for
surface mass balance to albedo. We aim to determine the range of ice albedo that occurs in the highest reaches of the glacier
and to what extent the observations from the stake network can be linked to albedo and the duration of ice exposure. Towards
this end, we compare in situ data and Sentinel-2 derived albedo, assessing whether the satellite imagery captures short-term
albedo variations and the seasonal variability of melt patterns. Finally, we consider the sensitivity of modeled surface mass

65 balance to observed albedo. The overarching objective is to contribute to a more comprehensive understanding of ongoing high
elevation glacier mass loss and the processes driving it, with an emphasis on the extreme summer of 2022 and the years since.

2 Data and Methods

2.1 Study site and instrumentation

Weißseespitze (WSS, 3518 m.a.s.l.) is a glacierized peak in the Ötztal range in western Austria and forms the high point of

70 Gepatschferner (Fig. 1). The summit region of WSS, above approximately 3480 m a.s.l., forms a small, dome-shaped cap
covering an area of about 0.05 km^2. Ice core analysis indicates that current surface ice at the site formed prior to the 1960s,
likely in the pre-industrial era, and that the age of the ice continuously increases with depth, reaching an age of 5.9 ± 0.7 ka
cal BP just above bedrock (Bohleber et al., 2020; Spagnesi et al., 2023). The ice in the summit region is cold based and ice
depths in the range of 8 m to 14 m were measured in the central part in 2018 (Fischer et al., 2022; Stocker-Waldhuber et al.,

75 2022b). Accordingly, an age range spanning millennia is condensed into only a few meters of ice at this location.

Gepatschferner as a whole is Austria's second largest glacier and covered an area of 15.5 km^2 in 2017 (most recent inven-
tory, Helfricht et al. (2024)). In the following, we focus mainly on the summit region around WSS (Fig. 1) and the (former)
accumulation area of Gepatschferner, which consists of a wide, low-angle basin above about 3100 m.a.s.l. Additionally, we
compute glacier-wide statistics to further contextualize the data from the summit region and accumulation area.

80 On October 31, 2017, an automatic weather station (AWS) was installed on the Weißseespitze summit ice cap at 3492 m
a.s.l. (Fig. 1). The AWS records air temperature and humidity (Rotronic-HC2S3), pressure (Vaisala PTB110), wind speed and
direction (Young-05103-45), up- and downwelling short- and longwave radiation (Hukseflux-NR01), distance to the surface
(Campbell Scientific SR50a), and ice temperatures (Campbell Scientific 225 temperature sensor string, 4 sensors at between 1
and 9 m depth at the time of installation). The sensor acquisition frequency is one observation per minute and data are logged

85 as 10 minutes averages. The station mast is drilled into the ice and requires periodic redrilling depending on ice ablation to
ensure the stability of the mast and roughly consistent sensor height above the ice surface. An automatic camera was installed

on January 31, 2018, on a rock outcrop about 130 m east of the AWS. The field of view of the camera encompasses the glacier surface between the camera and the AWS (Fig. 1, panel e). The AWS data are available on the pangaea repository along with information on sensor specifications (Stocker-Waldhuber et al., 2022a). The SR50 records contain considerable noise and a

90 data cleaning procedure was applied to extract surface height for sample periods (refer to supplementary material for more information on this).

2.2 Ablation stakes

Seven ablation stakes were drilled on the Weißseespitze summit ice cap between 2017 and 2019. Another stake was added in 2022. The maximum distance between the stakes is about 130 m and they are positioned at elevations between 3488 and

95 3506 m a.s.l. (Fig. 1, Fig. 2) The period of record for the stakes varies from one to seven summer seasons. Stake readings were carried out in irregular intervals two to four times per year. Observations include snow depth at the stake locations (if any) and changes of the ice surface relative to the stake. In most cases, the latter is a negative value referring to a decrease in surface elevation due to ice ablation. At some stakes and for some observational periods, the formation of superimposed ice causes slightly positive surface change. Following Geibel et al. (2022), we assume a reading uncertainty of ± 5 cm for ice ablation

100 measured at the stakes. We used a density of 900 kg m^{-3} to convert observed changes in the elevation of the ice surface to mass change (e.g. Cogley, 2011). Snow density was not measured and unless otherwise stated we consider only ice ablation in the following sections.

Stake positions were typically recorded with a Topcon HIPER V GNSS (Global Navigation Satellite System) receiver during the stake readings. Standard post-processing was applied to correct the raw data with the known location of reference stations.

105 Horizontal movement of the stakes due to ice flow is not apparent, in line with expectations for the site and previous findings (Bohleber et al., 2020). In the following, the positions of the stakes are given as the centroids of the GNSS coordinates recorded at the respective stakes between July and October over the years 2017 to 2024 (Fig. 2).

2.3 In situ albedo observations

Up- and downwelling shortwave radiation was measured with a Hukseflux-NR01 four component radiometer, which includes

110 two Hukseflux-SR01 sensors for the shortwave components. The SR01 is a second-class thermopile pyranometer as per the ISO 9060-1990 standard, with a field of view of 180°. Shortwave radiation from the up- and down-facing sensor pair (SW$_{in}$, SW$_{ref}$) was used to compute daily albedo values, i.e. a daily representation of bi-hemispherical reflectance (BHR, Schaepman-Strub et al., 2006). To minimise the influence of variations in illumination angle, daily albedo was calculated as the sum of reflected shortwave radiation per day divided by the sum of incoming shortwave radiation per day. To eliminate zero offset effects during

115 night time, SW$_{in}$ and SW$_{ref}$ values below 2 W m^{-2} were excluded from the albedo computation. In the following, "AWS albedo" refers to the daily BHR value as described above.

External factors affecting sensor performance and albedo are mainly related to snow or rime ice accumulation on the sensors. Riming is most common in winter during and immediately after storm periods. Instances of erroneously low albedo values in the winter months, when winter snow cover was present at the AWS site, were filtered based on thresholds and visual inspection
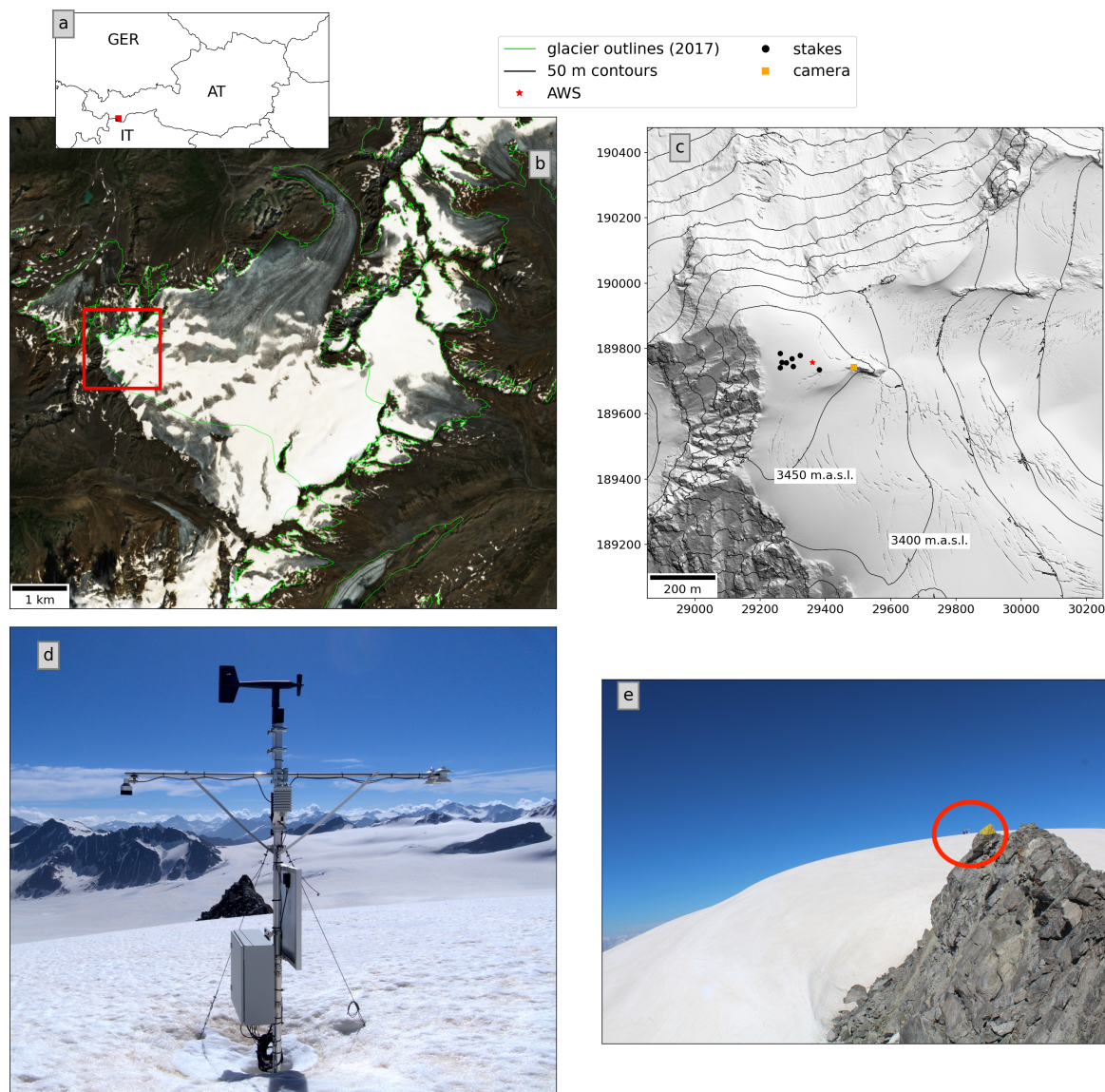
Figure 1. Panel a: Location of the study site in Austria. Panel b: Gepatschferner as seen in a Sentinel-2 scene acquired on 2021-08-14 with glacier outlines from the most recent regional glacier inventory (2017, Helfricht et al. (2024)). The red box indicates the subset shown in panel c. Panel c: Hillshade of the summit region with locations of the AWS, camera, and stakes. EPSG 31254, grid in metres. The hillshade and 50 m contour lines were derived from a digital elevation model for 2017 available from the geodata portal of the Tyrolean government (www.tirol.gv.at); elevations refer to orthometric heights. Panel d: The AWS as seen during a site visit on July 10, 2024. The automatic camera is mounted on the rock outcrop visible behind the AWS. Panel e: Image taken by the automatic camera on the same day. The field team can be seen next to the AWS (red circle).

120 of the camera imagery. Unrealistically low albedo values occur when, e.g., the downward facing sensor is fully or partially rime covered. Unrealistically high albedo values >1 can occur when snow or rime accumulates on the upward facing sensor, due to the slope and aspect of the underlying surface (e.g., Weiser et al., 2016; Picard et al., 2020; Bohn et al., 2024), a non-perfect cosine response of the upward-facing sensor, or surface roughness effects related to, for example, wind-produced features in the snow. Manual quality control was carried out for outlier data points by checking weather conditions in the camera images.

125 The instrument manual for the Hukseflux-SR01 (Hukseflux, 2023) outlines the evaluation of measurement uncertainty of the SR01 in accordance with the Guide to the expression of Uncertainty in Measurements (GUM, ISO 98-3) and indicates "achievable" measurement uncertainties of 6.2% in summer and 9.9% in winter for daily totals. To account for possible aging issues since calibration, we assume a relatively conservative uncertainty of 10% in the following for daily totals of up- and downwelling shortwave radiation, respectively. Based on standard error propagation for the ratio of up- and downwelling

130 radiation, we assume an uncertainty of 14% for the daily albedo.

Radiation measurements on glaciers can be affected by changing or unknown angles of slope and sensor tilt (e.g. Abermann et al., 2014; Weiser et al., 2016). The glacier surface at the WSS AWS is slightly sloped in a northeasterly direction, at an angle of around 6°-8° degrees as per a digital elevation model (DEM) derived from an airborne laser scanning survey carried out in 2017 (https://www.tirol.gv.at/sicherheit/geoinformation/geodaten-tiris/laserscandaten/, last access: 24 October 2024).

135 We discuss issues related to the sensitivity of daily AWS albedo to surface tilt angle in greater detail in the supplementary material (Fig. S1, S2). The estimated effect of the slope angle on albedo is an order of magnitude lower than the uncertainty associated with sensor accuracy and we therefore neglect more sophisticated corrections. We note that such corrections should be considered for assessments of sub-daily albedo (Weiser et al., 2016).

In the following, we refer to albedo below 0.40 as "low" and albedo below 0.20 as "very low". These categories are roughly

140 aligned with the 5% and 1% quantiles of the albedo time series. The threshold of 0.40 follows approaches by Fugazza et al. (2019) and Di Mauro and Fugazza (2022), who used this value to discriminate ice and snow. Glacier ice albedo below 0.20 occurs when the surface is loaded with organic and inorganic impurities or partially debris covered, and has been linked to the presence of liquid water (Paul et al., 2005; Di Mauro et al., 2017; Di Mauro, 2020; Rossini et al., 2023).

2.4 Sentinel-2 derived albedo

145 We used the Sentinel-2 (S2) harmonised surface reflectance product (Level-2A Drusch et al., 2012) to generate broadband surface reflectance estimates for the summit region of Weißseespitze and the overall glacier area of Gepatschferner. S2 data were obtained through Google Earth Engine (GEE, Gorelick et al., 2017). The S2 Scene Classification Layer band was used to remove pixels classified as saturated or defective. Cloud filtering was carried out using the Cloud Score+ product with a threshold of 0.5 in the cloud score band (Pasquarella et al., 2023). Multi-spectral reflectance was converted to broadband

150 reflectance using the conversion developed by Liang (2001), following prior work addressing broadband albedo of glacier surfaces (Naegeli et al., 2017). We omit corrections for the effects of reflectance anisotropy based on the results of Naegeli et al. (2017), who showed that the impact of such a correction is minimal for glacier albedo derived with the above approach.

We note that the derived quantity is not BHR but rather a hemispherical directional reflectance factor (HDRF, Schaepman-Strub et al., 2006). We use the term "S2-derived albedo" to refer to this in the following.

2.4.1 Point-scale S2-derived albedo

S2-derived albedo was extracted for the positions of the ablation stakes and the AWS for the period of record (2018-2024). To account for uncertainties in the stake positions, a 5 m buffer (Fig. 2) around the points was applied. Manual quality control was carried out to remove outliers and unreasonably low values in winter by comparing the point data with true color composites of the wider area. 5.2% of the cloud-filtered S2 data were discarded during this process due to cloud shadows and clouds not caught in the filter.

To relate ablation at the stake positions with albedo during the respective measurement intervals, the number of low albedo days per interval at each stake was estimated by augmenting the relatively sparse S2 time series with AWS data. We assumed that once low albedo values below 0.40 are reached at a given stake, albedo remains low until fresh snow brightens the glacier surface, and that a given snowfall brightens the surface at all stake positions and at the AWS. Hence, low albedo periods at the stakes were considered to begin any time the S2-derived albedo dropped below 0.40 at a given stake and to end if albedo at the AWS increased by at least 0.20 from one day to the next, indicating a brightening of the surface due to snowfall. The result is an estimated number of low albedo days at each stake for each measurement interval between consecutive stake readings.

2.4.2 Conditions during seasonal minimum snow cover

For an assessment of S2-derived glacier-wide albedo, we manually selected cloud free S2 scenes of Gepatschferner during conditions of minimum snow cover (2018-2024). We computed broadband albedo as described above for all snow and ice pixels within the glacier boundary. Non-ice and snow pixels containing debris cover and areas along the edge of the glacier tongue where the ice has retreated since the glacier outline was mapped were masked based on band ratio filters of NIR/SWIR1 and Red/SWIR1, similar to the approach of Paul et al. (2016). The GEE hillshadow function was applied based on the Copernicus 30 m DEM to mask terrain shadows, which are present on the lowest section of the glacier tongue. The upper parts of the glacier are not affected by terrain shadows. Mean S2-derived albedo was computed for the entire glacier area and for 20 m elevation bands.

2.5 Sensitivity experiments

To assess the sensitivity of the energy available for melt to albedo variations, we used the Coupled Snowpack and Ice Surface Energy and Mass Balance Model in Python (COSIPY, Sauter et al., 2020) to surface mass balance at the AWS location during periods of ice ablation between July and September. COSIPY requires air pressure, air temperature, relative humidity, incoming solar radiation, cloud cover or incoming longwave radiation, wind speed, precipitation, and optionally snowfall as input parameters. COSIPY version 1.4 was adapted to take albedo as an additional input parameter rather than applying the default albedo parameterization scheme. Aside from precipitation, the input was provided to the model as recorded by the AWS. Liq-
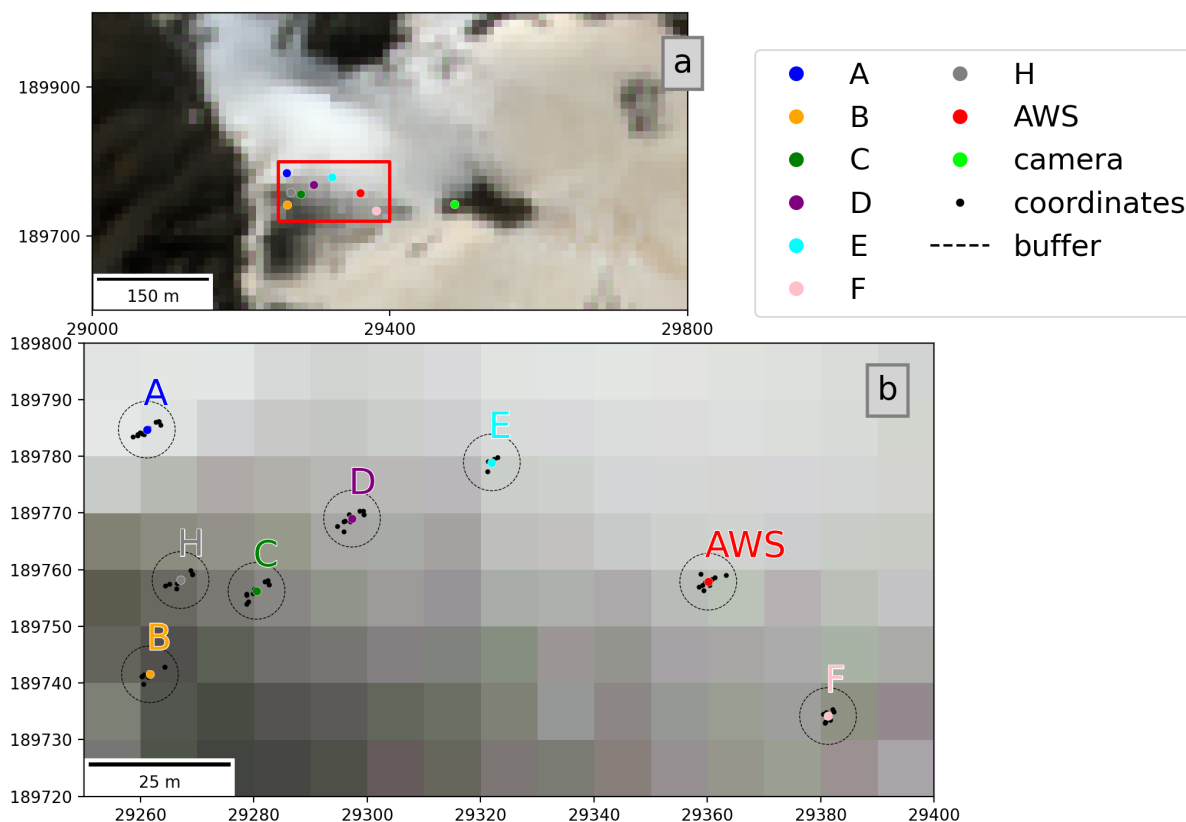
Figure 2. Positions of the AWS and the ablation stakes used in the following analyses plotted over a true color Sentinel-2 image acquired on 14 August 2021. Panel a: View of the summit area. The red box marks the subset shown in panel b. Panel b: Centroids of the stake positions (colored markers) with the GPS coordinates used to derive the centroids (black markers) and the 5 m buffer applied to extract the S2-derived albedo. All data are shown projected to the Austrian national grid (EPSG 31254, grid in metres).

uid precipitation is not available from the AWS and was set to zero as any parametrizations or lapse rate-based estimates would

185   introduce additional uncertainties (Klok and Oerlemans, 2002; Immerzeel et al., 2012). Snowfall was derived from surface height change for selected sub-periods (see supplementary material).

    We performed idealised sensitivity experiments to isolate the impact of albedo on melt in otherwise unchanged conditions by systematically varying albedo. We aim to highlight the influence of surface albedo on overall ablation, considering how "darker" vs. "brighter" bare ice influences mass balance, and how this varies with the time of year. For the idealised COSIPY

190   runs, albedo was kept constant over time and varied in increments of 0.05 for each run, i.e. each model run corresponds to one albedo value between 0.05 and 0.95. We did not consider energy balance processes related to seasonal or multi-annual (firn) snowpack.

Two experiments were performed: For a case-study focused on the 2022 season, we forced the model with meteorological input from a week-long heatwave in July 2022. For a more generalized assessment, the model was forced with "average" July-September conditions based on the 2018-2024 AWS time series. AWS records were grouped by time and day and averaged over all years. In both cases, we ran the model with the idealized, constant albedo as described above, and generated a control run with albedo as measured at the AWS.

Detailed validation exercises are beyond the scope of this study. However, running the model with input as recorded by the AWS for a sub period with SR50 data of acceptable quality shows good agreement between the modeled and measured surface height (Fig. S8, supplementary material) during the phase of snow melt and subsequent ice ablation at the station. The ability of the model to reproduce the observed height change during the transition from snow melt to a bare ice surface and ice ablation suggests that meaningful conceptualizations can be carried out with this approach.

3 Results

3.1 Time series of broadband albedo at WSS

3.1.1 In situ dataset

The glacier surface at the AWS location is snow covered most of the year and mean monthly albedo is around 0.80 from October to May. Mean monthly albedo drops to 0.71 in June, 0.64 in July, and 0.53 in August and increases again to 0.69 in September (Tab. 1). The standard deviation of albedo is higher in July, August, and September (0.14-0.20) compared to the rest of the year (0.10). August has the lowest mean albedo and highest standard deviation. 5% of all daily albedo values in the time series are lower than 0.46 and 1% are below 0.21.

Fig. 3 shows daily albedo anomalies compared to the time series mean. On average, a gradual albedo decline is apparent from late May until late August as seasonal snow ages or firn layers become exposed. A seasonal albedo minimum coinciding with a snow free ice surface at the AWS is typically reached during the second half of August. The subsequent increase in albedo is abrupt compared to the months-long decrease during snow melt, indicating the sudden, brightening influence of fresh autumn snow on the darker summer surface.

Annual minimum AWS albedo values were around 0.30 from 2018 to 2021 and occurred during periods with little or no remaining snow cover around the AWS (Fig. S4, supplementary material). From 2022 onwards, the minima were considerably lower, dropping below the previously observed range to 0.17 in 2022 and 2023 and to 0.16 in 2024 (Tab. 2).

2022 additionally stands out as the year with the earliest minimum and the longest period of low albedo values to date with 37 days of albedo lower than 0.40, including five days of albedo below 0.20. In previous seasons, the number of days below 0.40 ranged from three (2018) to eight (2020) and days below 0.20 did not occur. In 2023 and 2024, another five and six days of albedo below 0.20 were recorded, respectively (Tab. 2). The onset date of low and very low albedo conditions in 2024 cannot be determined due to an outage of the AWS in August; however, very low albedo conditions persisted into September, marking the latest recorded date of albedo values below 0.20 in the time series.
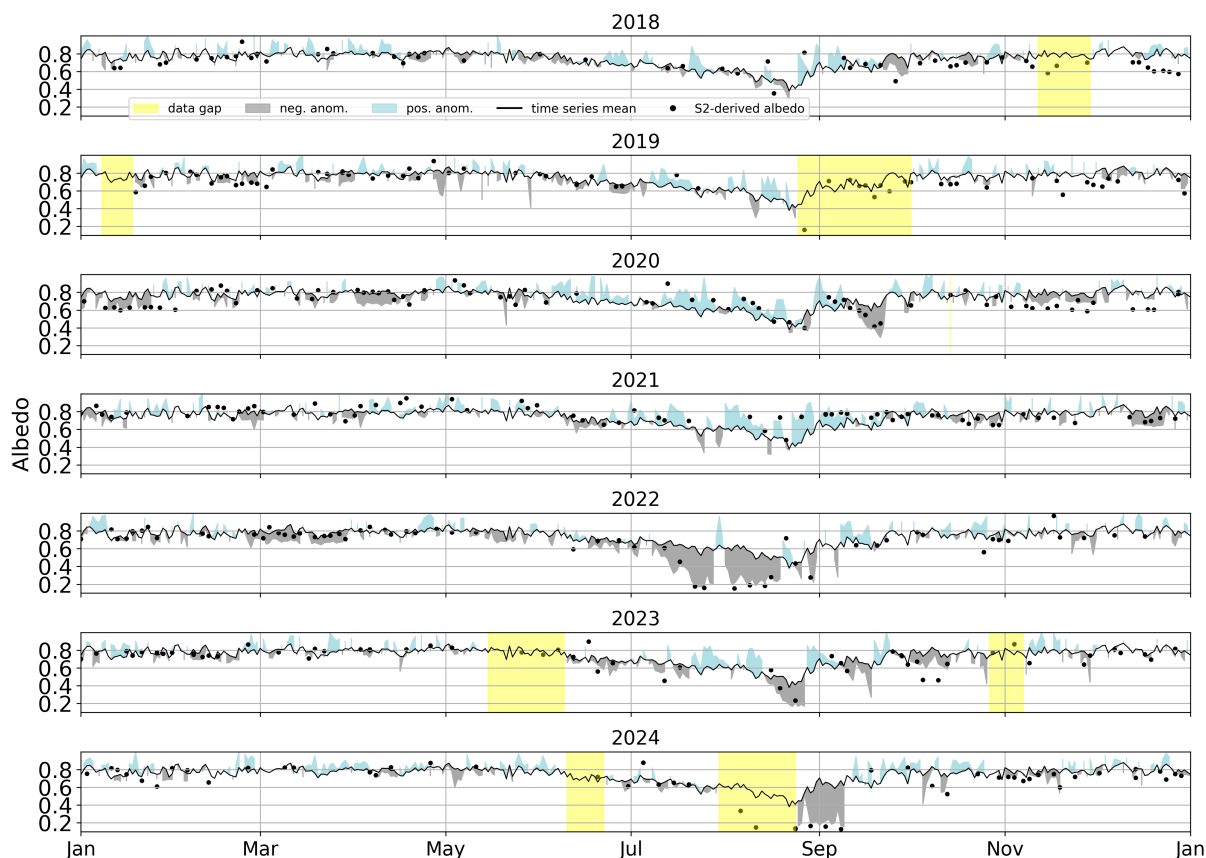
Figure 3. Daily albedo anomalies at the AWS for 2018-2024. Yellow shading marks major gaps in the time series due to instrumentation failures. The black line indicates the time series average. The blue and grey areas indicate daily albedo in the individual years as positive (blue) and negative (grey) anomalies from the time series average over all seven years. Black dots show Sentinel-2 derived albedo for the AWS location.

3.1.2 Sentinel-2 derived albedo

Comparing S2-derived albedo extracted for the AWS location with the in situ albedo shows good overall agreement (Fig. 4). The S2-derived albedo captures the pronounced low-albedo phases related to exposure of bare ice and the brightening events from snow fall (e.g. August 2022, Fig. 3). The absolute mean bias of the S2-derived albedo compared to the in situ data is 0.074 for all 412 data points shown in Fig. 4; the root mean square error (rmse) is 0.095. S2-derived albedo and AWS albedo agree well for the darkest bare-ice values around 0.20 with no apparent tendency for over- or underestimation (mean bias: 0.037, rmse: 0.041, N: 12), increasing our confidence that very dark bare-ice conditions in the WSS summit region are captured by the S2 acquisitions and not obscured by, e.g., mixed pixel effects.

Table 1. Monthly mean albedo and standard deviation at the AWS, 2018-2024.

Month	Mean	Standard deviation
Jan.	0.77	0.10
Feb.	0.78	0.10
Mar.	0.79	0.10
Apr.	0.79	0.08
May	0.80	0.10
Jun.	0.72	0.09
Jul.	0.64	0.14
Aug.	0.53	0.20
Sep.	0.69	0.17
Oct.	0.76	0.11
Nov.	0.78	0.10
Dec.	0.81	0.10

Table 2. Number of days per year with albedo below 0.40 and 0.20 ("below 0.40" is inclusive of days below 0.20), as well as the annual minimum values and the dates when the minima occurred.

Year	Days <0.40 (low albedo)	Days <0.20 (very low albedo)	Minimum	Date of minimum (mm-dd)
2018	3	0	0.207	08-22
2019	4	0	0.209	08-24
2020	8	0	0.209	09-20
2021	5	0	0.32	08-16
2022	37	5	0.17	07-24
2023	11	5	0.17	08-23
2024	15	6	0.16	09-08

S2-derived albedo at the stakes is greater than 0.56 in 90% of the cases shown in Fig. 5, and drops below 0.30 in 5% of cases. Low albedo periods in the S2-derived time series generally coincide with low albedo periods at the AWS and were observed in July (2022), August (2018, 2019, 2022, 2023, 2024), and September (2024). The earliest date of S2-derived albedo below 0.40 in the time series is July 22, 2022, indicating a very early start of the bare-ice period in the WSS summit region in 2022 in line with AWS data.

Low albedo periods in the S2-derived albedo dataset generally occur time synchronously at the various stake positions and the AWS location (Fig. 5). However, spatial variability of albedo in the WSS summit region is also apparent. For example, S2-derived albedo at stake B dropped to below 0.3 in the summer of 2021 while the other stakes and the AWS position retained
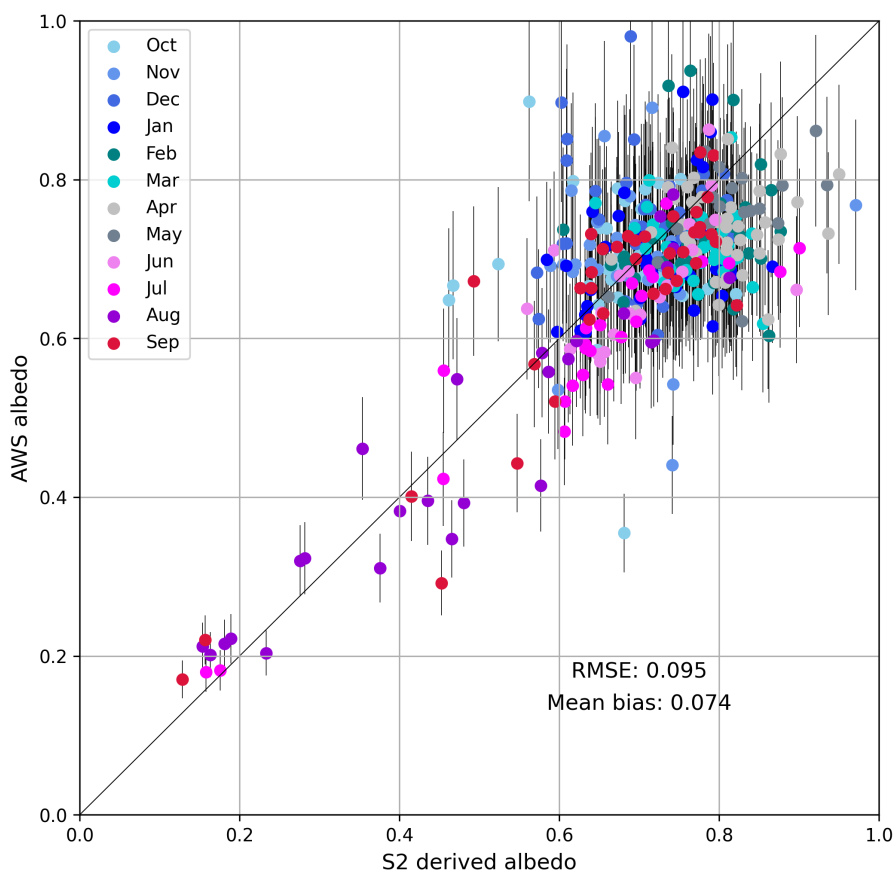
Figure 4. S2-derived albedo plotted against AWS in situ albedo from the same day, colour coded by month. Black vertical lines denote error bars for the in situ albedo based on the estimated uncertainty of 14%.

considerably higher albedo values. In summer 2018, S2-derived albedo at the AWS position dropped to slightly below 0.40 only once. In contrast, most stakes had low and even very low albedo values for multiple S2 acquisitions, indicating a longer period of exposed bare ice at the stakes than at the AWS, and hence the considerable small scale spatio-temporal variability of albedo.

245 **3.2 Albedo at the ablation stakes in the WSS summit region**

Ablation varies considerably between different stake positions on the small summit ice cap (Fig. 1, 2). Cumulative ice ablation over the melt seasons 2018-2023 was 1701 mm w.e. at stake A, while stakes B, C, and F lost 2799, 3069, and 3555 mm w.e., respectively. Stake F has the longest period of record, August 6 2017 to September 20 2024; cumulative ablation during this period was 5184 mm w.e. In the extremely warm summer of 2022, the four stakes mentioned above lost between 882 mm w.e.
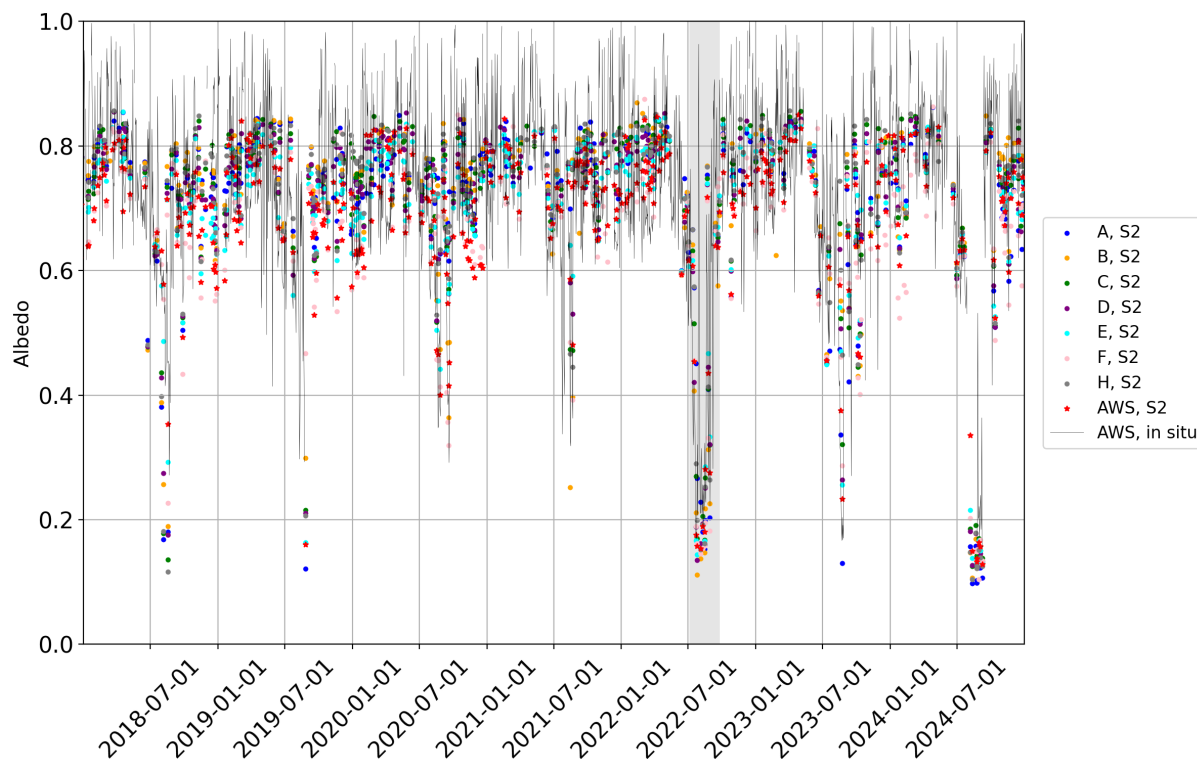
Figure 5. Sentinel-2 derived broadband albedo extracted for the stake locations and the AWS position. The thin black line shows daily albedo as measured in situ at the AWS. The grey shading indicates the temporal subset shown in more detail in Figure 7.

250   and 1521 mm w.e. of ice. During the more moderate summer of 2021, ablation values range from no ice ablation at stake A to 324 mm w.e. at stake B (Tab. 3).

Fig. 6, panel a, shows the estimated number of low albedo days per year at the stakes plotted against annual ablation. Estimated low albedo days per year range from zero to a maximum of 28 at stakes B and F in 2022 (Tab. 3). Annual mass loss tends to increase with the number of low albedo days. Conversely, low ablation values tend to occur in years with few low
255   albedo days. The Pearson correlation coefficient for ablation against the estimated number of low albedo days as shown in Fig. 6, panel a, is -0.8.

2018, 2022, and 2024 stand out as years with numerous low albedo days and high ablation values at the stake positions. For example, the estimated number of low albedo days was 22 in both 2018 and 2022 at stake A. Annual ablation at this stake was also very similar in both years with -855 and -882 mm w.e., respectively. At stake B, the estimated number of low albedo days
260   was 22 in 2018 but rose to 28 in 2022. Annual ablation at stake B was considerably higher in 2022 than in 2018 with -1521 mm w.e compared to -738 mm w.e. (Tab. 3).

The correlation apparent in the data is in line with expectations. However, the data contain outliers (e.g., no ablation and 20 low albedo days at stake D in 2018) and show a considerable range of ablation values for a given count of low albedo days.

For example, in cases with four estimated low albedo days, no ablation to losses greater than 650 mm w.e. were recorded
depending on the stake and measurement period (Fig. 6, panel a, Tab. 3)).

The outlier value at stake D in 2018 can be investigated further: Stake readings taken on July 31 and August 29 indicate there was no ice ablation at the stake position during this period. 97 cm of snow were recorded on July 31 at stake D, while neighboring stakes had zero remaining snow cover on this date. On September 27, 2 cm of positive ice surface height change were recorded at stake D. At stake C, the closest neighbor to stake D, the ice surface lowered by -85 cm (-765 mm w.e.) during the first period (July 31 to August 29). The second period (August 29 to September 27) saw a slightly positive surface elevation change (+4 cm) similar to stake D. Fig. S7 (supplement) shows impressions of the glacier surface in the WSS summit region during the stake readings on August 29, 2018. The key factor determining the diverging evolution at stakes D and C between July 31 and August 29 seems to be the considerable snow pack that was present at stake D in late July. In an S2 scene acquired on August 5, a strong albedo gradient associated with the transition from snow to bare ice can be seen in the vicinity of stake D (Fig. S6; refer to Sec. 4.1.2 for further discussion).

Fig. 6, panel b, breaks the ablation stake data down into individual measurement periods, showing the mean ablation rate during each period plotted against the percentage of estimated low albedo days in the same period. Low mean ablation rates tend to occur in measurement periods with few low albedo days. The highest mean ablation rates were reached in the measurement period with the highest amount of estimated low albedo days, in August 2018. Over 70% of the days between the stake readings on July 31 and August 29, 2018, were low albedo days at the positions of stakes A and B and both stakes reached mean ablation rates of over 25 mm w.e. per day. In 2024 (August 23-September 20), ablation rates between 22 and 24 mm w.e. per day were reached at stakes F and H, with 68% of this measurement period exhibiting low albedo days. August 4 to September 20, 2022, also stands out with high daily ablation rates between 16 and 19 mm w.e., although the percentage of low albedo days during the period was lower (38%-44% depending on the stake). In August 2019, similar mean ablation rates were reached at three stakes with only 12% of low albedo values during the measurement period.
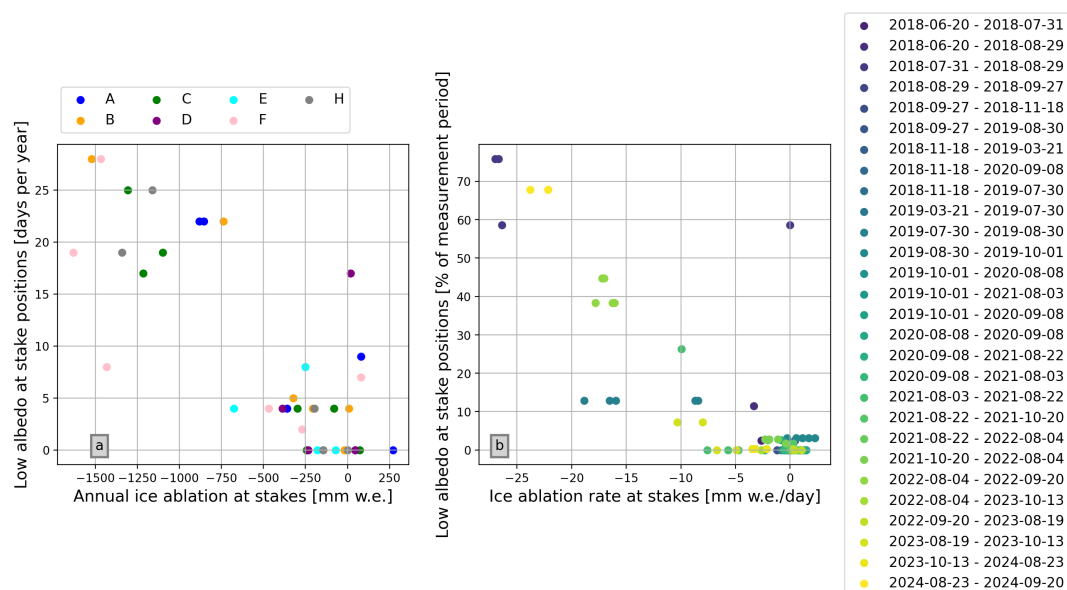
Figure 6. Panel a) Cumulative annual ablation at the stakes plotted against the estimated number of low albedo (<0.40) days per year at each stake position. Panel b) Ice ablation rate (ablation per measurement period divided by the length of the period) for each measurement period at the stakes plotted against the percentage of low albedo (<0.40) days at the respective stakes during the same measurement period.

Table 3. Estimated number of low albedo (<0.40) days derived from S2-data and the AWS time series and annual surface change (mm w.e.) at stakes A-H.

Year		A	B	C	D	E	F	H
2018	Low albedo days	22	22	20	20	8	8	22
	Ablation	-855	-738	-1215*	18	-252	-1431*	/
2019	Low albedo days	4	4	4	4	4	0	4
	Ablation	-360	9	-81	-387	-675	0	-198
2020	Low albedo days	0	4	0	0	0	7	0
	Ablation	45	-207	72	45	-72	81	0
2021	Low albedo days	0	5	0	0	0	2	0
	Ablation	270	-324	-243	-234	-180	-270	-144
2022	Low albedo days	22	28	25	25	25	28	25
	Ablation	-882	-1521	-1305	/	/	-1467	-1161
2023	Low albedo days	9	0	4	4	4	4	0
	Ablation	81	-18	-297	/	/	-468	-144
2024	Low albedo days	19	19	19	19	19	19	19
	Ablation	/	/	-1404	/	/	-1629	-1341

* : Drilled in 2017. 2018 value includes ablation between last reading in 2017 and first reading in 2018.

3.3 A closer look at summer 2022

Summer 2022 stands out as the first unusually dark year in the albedo time series and the period of low and very low albedo values is considerably longer than in all other years (Figs. 3, 5). In the following, we consider the low albedo period of 2022 in more detail to illustrate the characteristics of this exceptional season in the WSS summit region.

290   The AWS and S2 data show a relatively gradual decline of albedo from about 0.8 to under 0.20 from July 5 to July 22, 2022. This coincides with a period of increasing temperatures between July 7 and 22. Albedo at the position of stake A remained slightly higher compared to the other stakes due to lingering snow cover (Fig. 7 panel a, Fig. 8). Nighttime temperatures remained above freezing from July 13 to 28, when temperatures dropped and a small snowfall briefly brightened the surface. With the thin snow cover, albedo rose to over 0.9 at the AWS before dropping back to around 0.20 in early August. During

295   a stake reading on August 4, all stake positions were snow free. Albedo remained continuously low until another snowfall on August 19-20. This was followed by about five days of snow melt and darkening surfaces. Then, a series of small snowfalls followed by brief melt periods produced a rapid succession of low and relatively high daily albedo values. This short-term variation was not captured in S2 imagery due to cloud cover. In the second week of September, a more substantial snowfall brought a lasting brightening of the surface, marking the start of "snow season" in the summit region.

300   Ice surface elevation change at stakes A, B, C, and F between August 4 and September 20 ranged from -84±5 to -90±5 cm. Significant spatial variability of albedo between the stake locations is not apparent. The estimated number of days with low albedo values varies between 18 and 21. The satellite derived albedo at the stake locations suggests that stake A melted out a few days later than the other stakes (Fig. 7 panel a, Fig. 8) but this period was not captured by the stake readings. Considering the S2-derived albedo in Fig. 8, the ice of the WSS summit and the neighbouring ice-free areas show similar albedo values

305   between August 4 and 16, i.e. the ice was as dark as the surrounding rock.
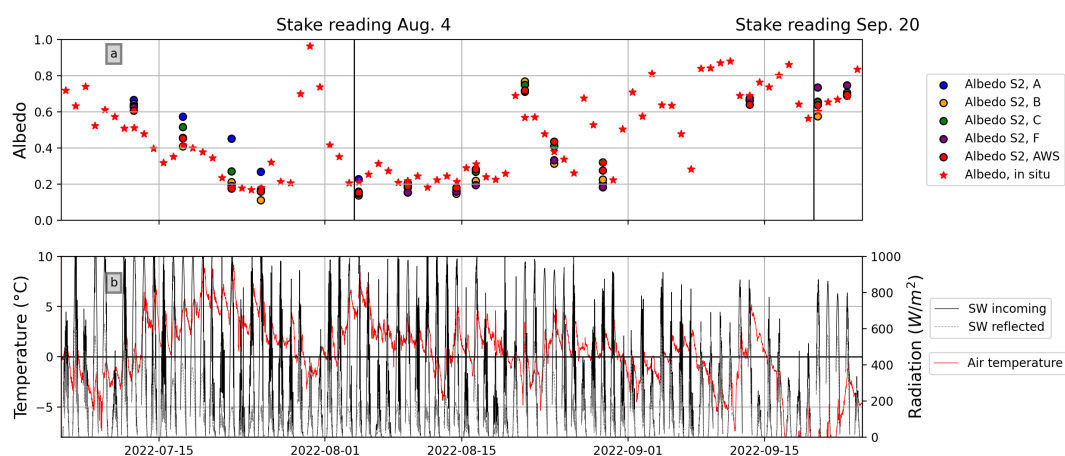
Figure 7. Panel a) Daily albedo at the AWS (red stars) from 2022-08-01 to 2022-09-01, and S2-derived albedo from cloud-free acquisitions during the same time period for the stakes shown in panel a. Panel b) Air temperature (red line) and shortwave radiation (black line: incoming, grey line: reflected) at the AWS.
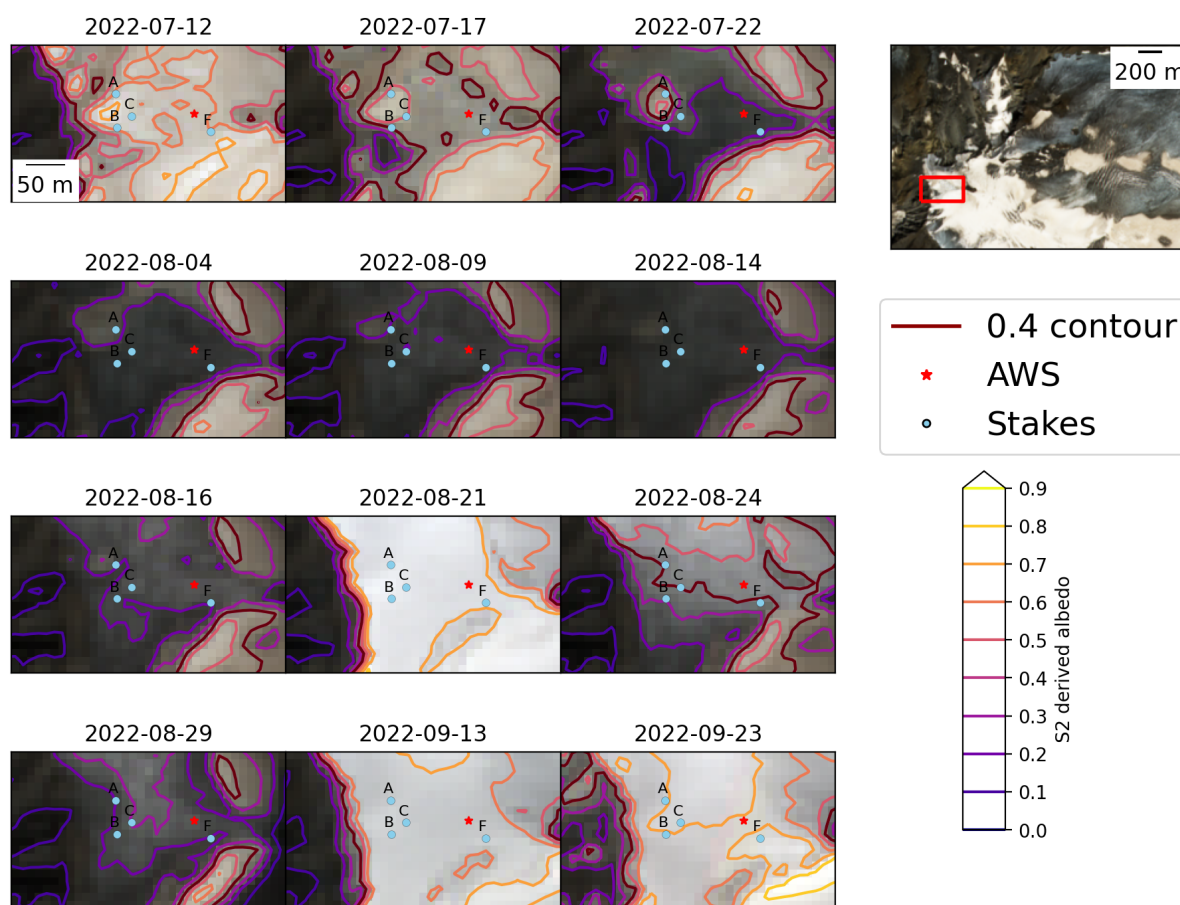
Figure 8. RGB composites of cloud free S2 scenes of the Weißseespitze summit region acquired between July 12 and September 23, 2022. The location on the glacier is shown in the inset in the top right (larger crop of the 2022-07-17 scene). The scenes correspond to the point values of broadband albedo as shown in Fig. 7. The positions of the AWS and the stakes listed are marked in red and grey, respectively. The contour lines indicate S2 derived albedo, the 0.40 contour is highlighted in dark red.

3.4 Sensitivity of surface mass balance to albedo

3.4.1 Experiment 1: 2022 heat wave

Fig. 9, panel a, shows air temperature and incoming radiation during a week of very warm, sunny weather that preceded the albedo minimum in July 2022 (see also Fig. 7, Fig. 8). Modeled surface mass balance (SMB) is shown for albedo as measured
310 at the AWS and for model runs with a range of constant albedo values (Fig. 9, panels b, c). Daily cycles of SMB during cloud free conditions are predominantly driven by incoming solar radiation. If clouds are present (e.g., July 20 - July 21), the influence of long wave radiation and latent heat flux on SMB is more apparent. On July 17 and 18, measured albedo was around 0.40 and modeled daily SMB amounts to about -36 mm w.e. On July 22, albedo dropped to very low values around 0.20 and daily SMB almost doubled to -71 mm w.e.. Considering the entire week-long heatwave, total modeled surface mass
315 loss increases by about 50 mm w.e. if albedo is decreased by 0.1. Total modeled SMB for the week amounts to -302 mm w.e. in the "low albedo" (0.40) scenario and to -407 mm w.e. in the "very low albedo" (0.20) scenario. Total SMB for albedo as measured at the AWS is -337 mm w.e.
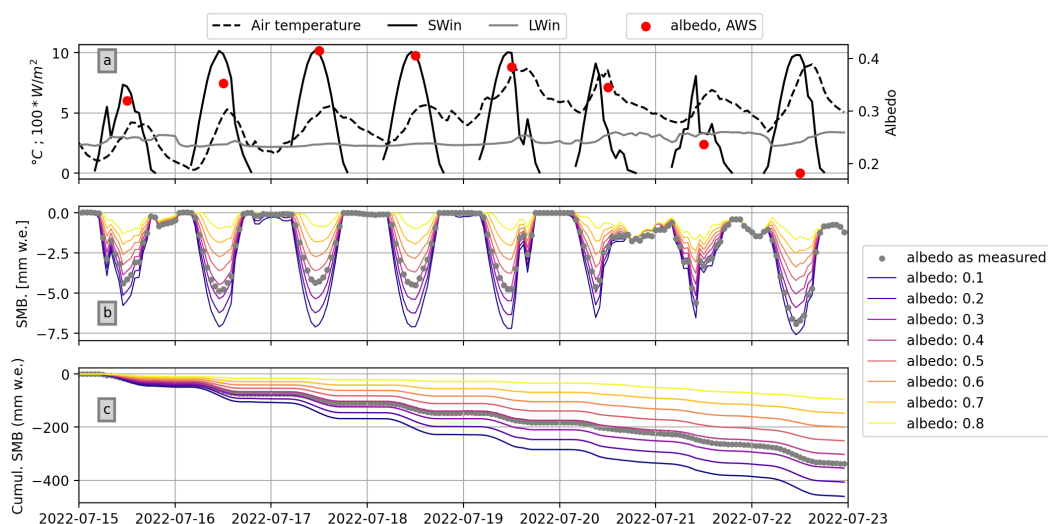
Figure 9. a: Incoming short- and longwave radiation, air temperature, and albedo as measured by the AWS during the July 2022 heatwave. b: Modelled surface mass balance (SMB) with albedo input as measured and varied at constant levels. c: Cumulative surface mass balance for the week, albedo input as in panel b.

3.4.2 Experiment 2: Average seasonal forcing data and varying albedo

Low albedo values and bare ice conditions at the AWS occur between July and September (Fig. 3). Forcing COSIPY with
320 average July-September input generated from the 2018-2024 time series and varying only albedo indicates that the impact of low and very low albedo is greatest early in this three-month period and decreases as the season progresses and incoming solar
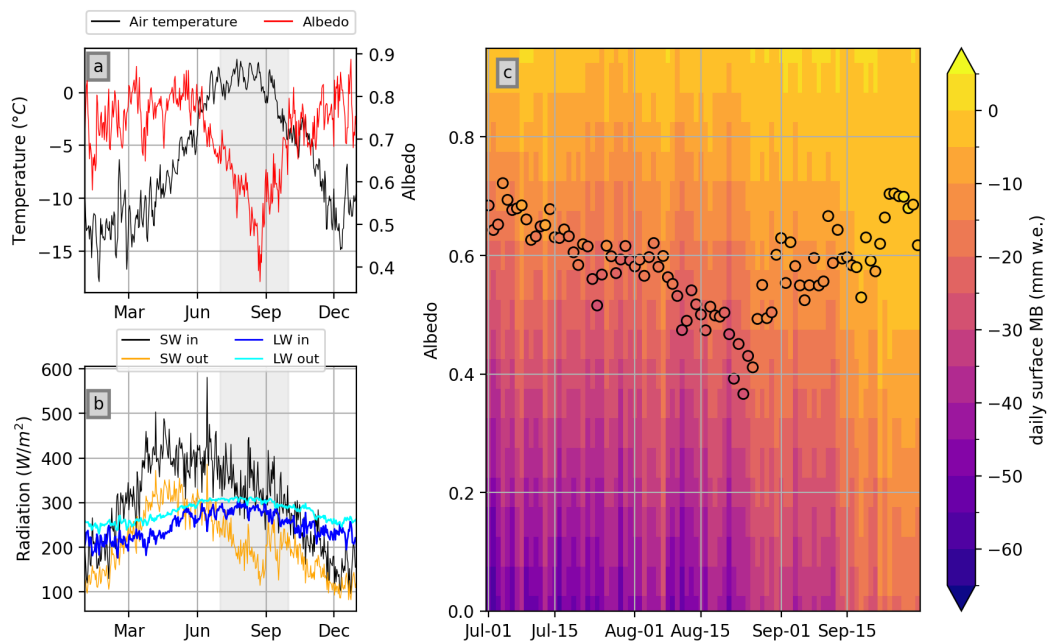
Figure 10. a: Daily air temperature and albedo averaged over the 2018-2024 AWS time series. b: Daily mean radiation (short- and longwave, up- and downwelling) averaged over the 2018-2024 AWS time series. Grey shading indicates July 1 to Sep 30, as shown in panel c. c: Modeled daily surface mass balance using the 2018-2024 averages as model input. The circular markers indicate albedo as measured (as in panel a). The background mesh shows modeled mass balance for albedo that is constant in time over the July 1 to Sep. 30 period, varied in increments of 0.05.

radiation decreases (Fig. 10, 11). Average modeled daily surface mass loss in low (very low) albedo conditions is 10 (13) mm w.e. greater in July than during the first half of September. On an average July day on Weißseespitze, bare ice with an albedo of 0.20 is associated with a mean surface mass loss of 38 mm w.e. By late September, the same very low albedo is associated with about 20 mm w.e. of mass loss. The modeled seasonal differences in daily SMB are more pronounced in very low albedo scenarios compared to higher albedo. For an albedo of 0.1, the difference between early July and late September is 25 mm w.e. For albedo values of 0.40 and 0.60, the difference decreases to 19 mm w.e. and 13 mm w.e., respectively (Fig. 11).
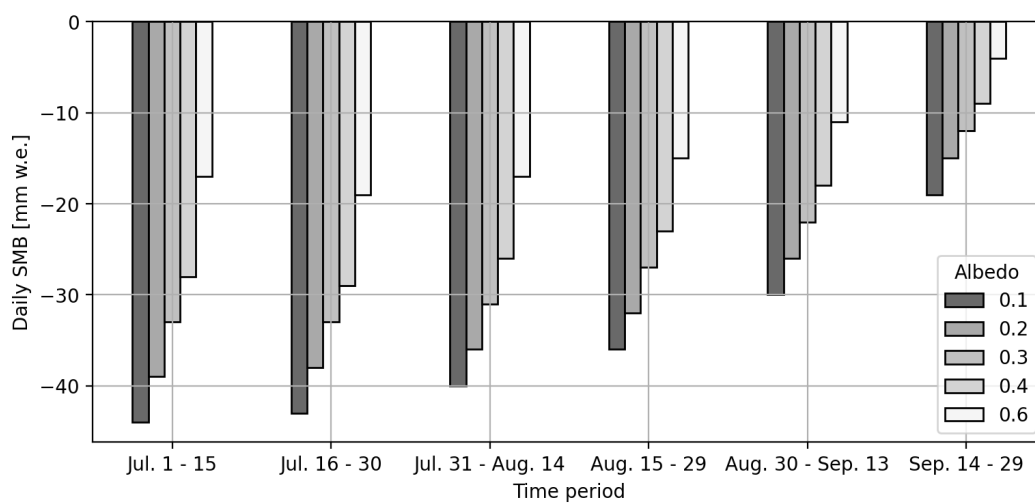
Figure 11. Meam modelled daily SMB over 15 day time periods of average July-September conditions and different albedo values. Refer to Table S1 in the supplement for a tabular version of this data.

3.5 Interannual elevation dependent albedo variability

To expand the analysis from the summit region of Weißseespitze to the scale of the entire glacier, Fig. 12 shows S2 scenes
330   acquired around the time of the seasonal snow cover minimum for 2018-2024 (panels a-f) with corresponding S2-derived
albedo binned by elevation bands (panel i). Albedo is very low in the ablation zone up to about 2850 m a.s.l. in all years.
Interannual variability increases at higher elevations as snow cover in the (former) accumulation zone varies. In the highest
regions of the glacier above 3200 m a.s.l., 2022, 2023, and 2024 stand out as darker than previous years and only very limited
sections of Gepatschferner remained snow covered.

335   In the 2022 and 2024 scenes, an extremely dark area is noticeable in the central upper section of the glacier (Fig. 12). The
albedo of the ice surface drops below 0.20 here. An albedo contour line of 0.15 captures the outline of the visually darkest area
well and emphasizes the decrease of albedo even beyond the "very low" (<0.2) albedo of the surrounding ice surfaces (Fig.
12, panel h). Similarly dark ice surfaces close to the snow or firn line are also found in 2018 and, to a lesser extent, in 2023.
In histogram visualizations (Fig. 13) of the S2-derived albedo for the scenes shown in Fig. 12, snow cover and bare ice areas
340   are apparent as bi-modal histogram peaks around 0.5-0.6 and 0.20, respectively, from 2018 to 2021. Glacier wide mean albedo
ranged from 0.28 in 2018 to 0.41 in 2021. In 2022 and 2024, glacier wide mean albedo dropped to 0.22 and the remaining
snow cover did not form a distinct peak, resulting in a uni-modal albedo distribution. 20% and 22% of the glacier area had
albedo values below 0.15 in 2022 and 2024, respectively. Most of these very dark areas are concentrated in the relatively high,
central section of the glacier mentioned above. 2018 and 2023 similarly have very small secondary peaks, highlighting that a
345   bi-modal albedo distribution separating accumulation and ablation area does not hold in extreme melt years once multi-year
firn is depleted. Albedo values for snow free glacier surfaces range from 0.10-0.15 to around 0.40, underlining the considerable
variability of bare-ice albedo particularly at high elevations (Figs. 12, 13).
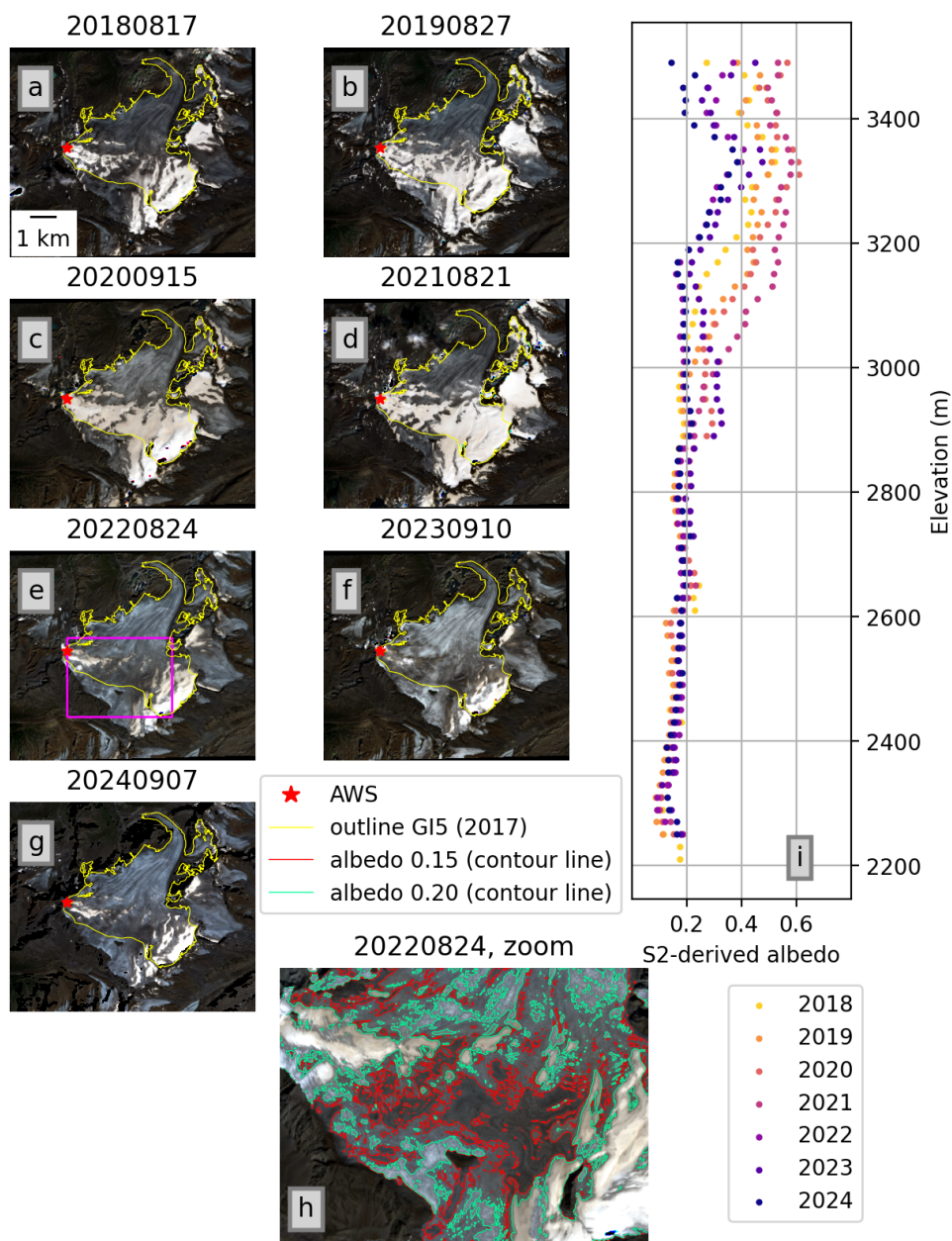
Figure 12. a-g: True color composites of Gepatschferner around the time of the seasonal snow cover minimum for 2018-2024. i: Mean albedo per 20 m elevation bands for the same six scenes as in a-f. h: subset of the 2022 scene shown in panel e (magenta box) with contour lines for S2-derived albedo <0.15 and <0.20.
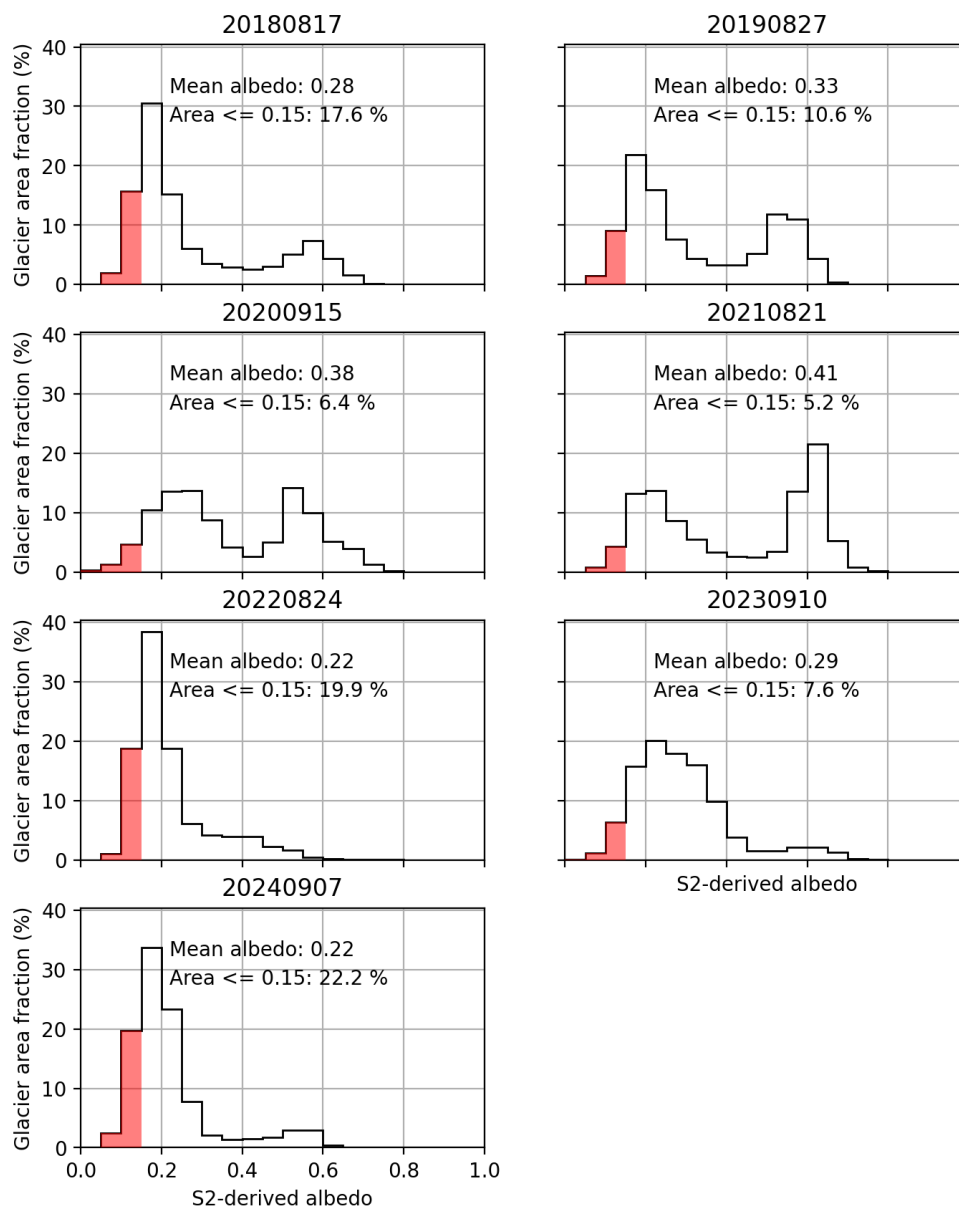
Figure 13. Histograms of S2-derived albedo in relation to glacier area for S2 scenes acquired around the time of the seasonal snow cover minimum from 2018-2024, as shown in Fig. 12. Area with albedo below 0.15 is highlighted in red; annotations show glacier-wide mean albedo for each scene.

4 Discussion

4.1 Method-related limitations

350 #### 4.1.1 S2-derived albedo and comparison with in situ albedo

Generating an approximation of broadband albedo from S2 data over ice surfaces involves a number of challenges, which have been addressed in detail by previous studies. Our approach follows Naegeli et al. (2015, 2017), who found that the narrow-to-broadband conversion of Liang (2001) is suitable for ice albedo. Naegeli et al. (2017) further showed that the effect of BRDF corrections on ice albedo is negligible. Likewise, the effects of atmospheric corrections have been shown to have only a minor
355 impact on satellite-derived glacier albedo (Fugazza et al., 2016; Traversa et al., 2021).

In the spatial dimension, the main assumptions underlying our analyses are that the locations of the stakes and AWS in relation to the S2 grid can be determined with enough accuracy to allow a comparison, and that mixed pixel effects are relatively small. The GNSS coordinates (Fig. 2) indicate that the locational uncertainty of the point positions is considerably smaller than the pixel size of the S2 grid. We assume the 5 m buffer applied during the extraction of the S2-derived albedo (section 2.4.1)
360 sufficiently captures the true location of the stakes. We note that the S2 grid is also subject to geometric uncertainties. Pandžic et al. (2016) found a potential offset of about 6 m or 0.6 pixels between S2 imagery and an Austrian regional high resolution DEM. The correlation between in situ albedo as measured at the AWS and S2-derived albedo at the AWS position does not change substantially for a 5 m buffer versus a 10 m buffer, hence we consider the 5 m buffer adequate (mean bias 0.076 with 10 m buffer vs. 0.074 with 5 m buffer).

365 #### 4.1.2 Estimated number of low albedo days

We highlight that the estimated number of low albedo days as described in section 2.4.1 is indeed an estimate and should be interpreted with caution. The AWS times series allows us to assess how the estimated number of low albedo days generated from the S2-derived albedo at the AWS location compares with the observed number (Tab. 4). An underestimation of calculated low albedo days compared to the observation is to be expected in cases when albedo drops below the threshold of 0.40 at the
370 AWS and S2 data is not immediately available, or when the S2 time series misses short periods of low albedo entirely. In all years except 2018 and 2024, the expected underestimation occurs or the estimate of low albedo days matches the observation (Tab. 4).

In 2024, the observation does not capture the true number of low albedo days due to the prolonged data gap in August. In 2018 there is no such gap, yet the estimated number of low albedo days (8) at the AWS is greater than the observed number
375 (3). When comparing ablation with the number of low albedo days at the stakes in 2018 (Fig. 6, Tab. 3), stake D also presents a noticeable outlier with 20 low albedo days and no ice ablation. In contrast, neighboring stake C had the same number of low albedo days and more than 1 m w.e. of ice loss. This indicates that the linkage between ablation and albedo was not well captured by the S2 data in 2018 for at least some of the stake positions and the AWS. Anecdotally, spatially variable snow

Table 4. Estimated number of low albedo days derived via the combined S2 and AWS datasets (Sec. 2.4.1) for the AWS location compared to the number of low albedo days derived from in situ data measured at the AWS.

Year	S2-derived estimate of low albedo days	Low albedo days in AWS time series
2018	8	3
2019	4	4
2020	0	8
2021	0	5
2022	25	37
2023	9	11
2024	19	14

depth has often been observed in the WSS summit region during site visits. It seems likely that the 2018 discrepancies at stake
380 D are related to small scale variations in the snow melt pattern that were not resolved in the S2 data.

In 2018, low (<0.40) albedo in the S2-derived time series first occurred on August 17. The albedo observed in situ on the same day was 0.45. The "low albedo" threshold was crossed four days later, on August 21. Observed in situ albedo fluctuated somewhat in the following days, resulting in three days of "low albedo" before a snow fall event brightened the surface on August 25 (Fig. S6, supplement). Taking into account the assumed uncertainty of ±14% in the daily in situ albedo
385 (Sec. 2.3), it is apparent that the "low albedo days" identified in the S2-derived estimate were within uncertainty of the "low albedo" threshold in the in situ data. This highlights the limitations of categorical threshold choices as well as the considerable uncertainty in the daily albedo observations.

4.2 Albedo and ablation at Weißseespitze

The WSS datasets show the strong albedo impact of snow and firn loss in the upper-most elevations (>3000 m) of Gepatschferner,
390 one of Austria's largest and highest glaciers. Distinct periods of low or very low albedo are clearly apparent in the in situ and S2-derived albedo. In addition to albedo variability related to snow vs. ice surfaces, bare ice albedo in the former accumulation zone also varies spatially and from year to year. Ice albedo can reach values as low as those of the surrounding rock in "dark years" (Fig. 8).

All else remaining equal, the difference in ablation between relatively bright bare ice surfaces with albedo values around
395 0.40 and extremely dark surfaces with albedo below 0.15, as seen in 2022 and 2024 (Figs. 12, 13), is on the order of 10-15 mm w.e. additional daily surface melt for average July-September conditions at WSS (Fig. 11). These sensitivities of SMB to albedo are similar to findings by comparable studies at lower elevations (e.g. Oerlemans et al., 2009; Naegeli and Huss, 2017; Barandun et al., 2022). Naegeli and Huss (2017) showed a decrease of glacier wide mass balance by -0.14 m w.e. per year per 0.1 albedo decrease in a study assessing the period 1997 to 2016 for 12 glaciers in Switzerland. They found the greatest
400 influence of albedo changes at the glacier terminus and no impact in the accumulation area, which they note to be snow-covered

year-round and thus not sensitive to bare ice albedo variability (Naegeli and Huss, 2017), in line with findings by Oerlemans et al. (2009). The WSS dataset exemplifies that sensitivity of SMB to albedo change can in fact be very pronounced in (former) accumulation zones as periods of bare ice become longer and occur more frequently. SMB sensitivity to albedo in the summit region of WSS is in the range of Naegeli and Huss (2017)'s results for the lower sections of their study sites.

405   Besides the absolute albedo of the glacier surface, the amount of time the dark, bare ice is exposed and when in the season this exposure occurs are also key controls of ice ablation on the small summit ice cap of WSS. The observational data show that ice loss at the stakes increases with the amount of low albedo days (Fig. 6). Snow melt patterns in the WSS summit region vary from year to year, which can lead to small scale variability of ablation between the stakes due to the varying length of ice exposure. This snow-driven variability decreases in extreme melt years when the summit region is completely snow free, such

410 as 2022 and 2024. The length of the observed low albedo periods in the time series range from 37 days (2022) to 3 (2018). Assuming average August conditions and an albedo of 0.35, the modeled SMB for 37 days amounts to -962 mm w.e. versus -78 mm w.e. for 3 days. This range is broadly aligned with observed ablation for seasons with long and shorter low albedo periods (Tab. 3). Very low albedo was observed at the AWS on 5 to 6 days per year from 2022 onward. 5 days with an albedo of 0.20 result in 31% more modeled ice loss if they occur in late July, like in 2022, rather than early September like in 2024

415 (-190 mm w.e. vs. -130 mm w.e.). Given the ice depths of 8 to 14 m measured in the summit region in 2018, we note that the ablation season of 2022 alone is likely to have caused the loss of around 7 to 12 % of remaining ice thickness.

4.3   Open questions: Drivers of very low albedo conditions

The mostly continuous seven-year AWS time series from WSS shows considerable temporal variability in the seasonal albedo minima, with exceptionally low values below 0.20 observed since 2022. At the glacier scale, 2022 and 2024 stand out as

420 very low albedo years. Possible explanations for the darkened ice surface in these particular years include the presence of organic and inorganic impurities and stagnant melt water (e.g. Oerlemans et al., 2009; Di Mauro et al., 2017; Di Mauro, 2020; Di Mauro et al., 2020; Barandun et al., 2022; Gilardoni et al., 2022), and may additionally be related to the hydrology and state of the weathering crust (e.g. Takeuchi et al., 2001; Cook et al., 2016; Tedstone et al., 2020; Traversa and Di Mauro, 2024). Reduced nighttime refreezing of supraglacial meltwater during heatwave conditions (e.g., in summer 2022) may have

425 contributed to the very low albedo values in the summit region. The terrain in the upper section of Gepatschferner where summer minimum conditions in 2022 and 2024 were extremely dark (Fig. 12) forms a slight depression where meltwater can pool until new channels are formed that allow it to drain. Based on the S2 imagery, it appears that the dark areas in the upper regions of the glacier were related to impurities that remained and accumulated on the ice surface after snow, firn, or ice layers melted, and to the presence of liquid water. This process has previously been observed in analyses of an ice core drilled in the

430 accumulation zone of the Adamello glacier (Garzonio et al., 2018). In addition to the presence of water as such, organic or inorganic impurities on the glacier surface appear darker if wet, affecting surface albedo.

    Ice cores from the Weißseespitze summit ice cap show distinct peaks of micro-charcoal in near-surface layers (Spagnesi et al., 2023). In a core drilled in 2021, the upper-most 50 cm of ice in particular have high micro-charcoal concentrations (Fig.3 in Spagnesi et al., 2023). Given the ablation records from the stakes, it is likely that this layer partially or completely melted

435   in 2022, exposing ice with higher impurity content and/or causing impurities that were contained in the ice to accumulate on the surface, thus potentially darkening the ice. At present, the linkage of surface albedo and impurities in the cores is intriguing but speculative, pointing to the limitations of broadband albedo for detailed surface type characterization. Resolving the spectral signature of the ice surface via remote sensing imaging spectroscopy or in situ spectroradiometric measurements in combination with targeted sampling of surface layer ice could provide further insights.

440   This relates to the need for fine-grained surface classifications at the glacier scale that account for the spatial variability in bare ice albedo, as mentioned above. Interdisciplinary studies combining in situ observations and remote sensing at increased spectral and spatial resolution with modeling are needed to improve understanding of the drivers of bare ice variability (Zhang et al., 2018; Gilardoni et al., 2022; Barandun et al., 2022; Bonilla et al., 2023).

4.4   What does the future hold?

445   Temperature index based mass balance modeling suggests that Gepatschferner will lose about 95% of its 2017 volume by the end of the century in a future scenario where warming levels are limited to 1.5°C above pre-industrial temperatures; in a 2°C scenario, practically all ice is lost before 2100 (Hartl et al., 2024a). In the projections, ice is retained longest in the uppermost regions of the glacier (Fig. 8 in Hartl et al., 2024a), including the area of very low albedo in the former accumulation zone discussed above (Fig. 12).

450   As firn loss progresses, albedo sensitivity and variability in bare ice albedo will become increasingly important at the highest elevations of Alpine glaciers. At Gepatschferner, multi-year firn has effectively disappeared. Imagining future summer seasons on Weißseespitze and Gepatschferner based on the 2018 to 2024 observations, it is likely that annual mass balance gradients and glacier-wide as well as distributed albedo will be defined by seasonal snow cover and short term brightening of the upper regions by summer snow falls rather than by the bi-modal divide between the ablation and accumulation zones that was 455   previously a key characteristic of the glacier system. Conditions as described for the extreme summer of 2003 (Paul et al., 2005) have occurred annually since 2022 at Gepatschferner. Future years may see more winter snow or cooler summers than in the past three years, but Gepatschferner no longer has a consistent or persistent accumulation zone and hence cannot be expected to survive in the current climate or under future warming conditions (Pelto, 2010, 2011).

    In the projected evolution of Gepatschferner mentioned above, ice surface conditions and the possible range of bare ice 460   albedo are not taken into account. Considering specifically the very dark zone in the upper section, one might imagine a prolonged period of ice exposure of, for example, 20 days in a near-future summer. In our COSIPY experiment for average July through September conditions (Section 3.4.2), modeled SMB for 20 days amounts to -268 mm w.e. for an albedo of 0.6, a typical value for aged snow. For a relatively bright ice surface with an albedo of 0.40, modeled SMB amounts to -438 mm w.e. For very dark ice with an albedo of 0.15, modeled SMB is -655 mm w.e. If the dark ice surface persists in 465   the same area over multiple years, as it has done at Gepatschferner, the reduced albedo will increasingly affect the spatial patterns of ablation in ways that elevation dependent mass balance gradients do not capture, increasing uncertainties in model projections. Mass balance models that do not resolve albedo variability and the occurrence of very dark ice surfaces may considerably underestimate melt particularly at high elevation in former accumulation zones. Deglaciation may occur sooner

than anticipated by current projections if melt-albedo feedback processes are not resolved in modeling efforts. We concur with previous studies that have highlighted the need for improved albedo parametrizations and assimilation of albedo observations in mass balance modeling (e.g. Paul et al., 2005; Naegeli et al., 2015; Naegeli and Huss, 2017; Draeger et al., 2024).

5 Conclusions

Ice ablation in the summit region of Weißsseespitze is strongly linked to the duration and timing of bare ice exposure. The length of the seasonal low (<0.40) and very low (<0.20) albedo periods in the former accumulation zone reached a new record in 2022 with 37 days of ice exposure. The absolute albedo dropped from seasonal minima around 0.3 to 0.17 in 2022 and did not recover in 2023 or 2024. This suggests increased impurity content at the ice surface since 2022, for example due to impurities previously contained in recently melted ice layers accumulating on the surface, changes to the weathering crust, more supraglacial melt water, or a combination of these factors. Sentinel-2 derived albedo captures the sub-seasonal range of albedo observed in situ well and provides valuable spatial context on seasonal snow melt patterns. Gepatschferner has effectively lost its accumulation zone. Albedo below 0.15 was observed on more than 20% of glacier area in 2024 and the largest very dark sections are found at relatively high elevations, in the former accumulation zone. In future summers, seasonal snow and the spatial variability of bare ice albedo will play a key role for melt patterns. To improve understanding of the driving processes governing ice albedo variability in space and time, multi-disciplinary research that integrates different data and sensor types with modeling approaches is needed. Accurate sub-seasonal and spatially explicit albedo characterizations are essential for improved projections of future glacier evolution as we shift from glaciers defined by albedo and mass balance gradients aligned with the ablation and accumulation zones to glaciers that no longer retain any multi-annual firn and do not have consistent accumulation zones.

Data availability. The stake readings and an up-to-date version of the of meteorological data from the AWS have been submitted to the pangaea data repository and will be freely available once the data curation process at pangaea is complete. The AWS data for 2017-2021 are available at Stocker-Waldhuber et al. (2022a) (https://doi.pangaea.de/10.1594/PANGAEA.939830). This data publication will be updated through 2024.

Author contributions. LH, KN, and FC conceptualized the study. MS maintains the AWS and ablation stake network at the study site and contributed to data curation. AB contributed to AWS data curation and energy balance modeling (methodology and software). DF and BD advised on methodology. LH implemented the formal analysis, produced visualizations, and wrote the original draft. All authors reviewed and edited the draft.

Competing interests. We have no competing interests to declare.

Acknowledgements. L. Hartl is funded by the Austrian Science Fund (FWF) grant number 10.55776/ESP250. A. Baldo and M. Stocker-Waldhuber received funding from FWF grants 10.55776/P34399 and 10.55776/I5246, which also contributed to the installation and maintenance of the instrumentation at WSS. K. Naegeli is supported by the ESA PRODEX Trishna T-SEC project (PEA C4000133711).

References

Abermann, J., Kinnard, C., and MacDONELL, S.: Albedo variations and the impact of clouds on glaciers in the Chilean semi-arid Andes, Journal of Glaciology, 60, 183–191, 2014.

Azzoni, R. S., Senese, A., Zerboni, A., Maugeri, M., Smiraglia, C., and Diolaiuti, G. A.: Estimating ice albedo from fine debris cover quantified by a semi-automatic method: the case study of Forni Glacier, Italian Alps, The Cryosphere, 10, 665–679, 2016.

Barandun, M., Bravo, C., Grobety, B., Jenk, T., Fang, L., Naegeli, K., Rivera, A., Cisternas, S., Münster, T., and Schwikowski, M.: Anthropogenic influence on surface changes at the Olivares glaciers; Central Chile, Science of the Total Environment, 833, 155 068, 2022.

Berthier, E., Vincent, C., and Six, D.: Exceptional thinning through the entire altitudinal range of Mont-Blanc glaciers during the 2021/22 mass balance year, Journal of Glaciology, pp. 1–6, 2023.

Bohleber, P., Schwikowski, M., Stocker-Waldhuber, M., Fang, L., and Fischer, A.: New glacier evidence for ice-free summits during the life of the Tyrolean Iceman, Scientific Reports, 10, 20 513, 2020.

Bohn, N., Bair, E. H., Brodrick, P. G., Carmon, N., Green, R. O., Painter, T. H., and Thompson, D. R.: The pitfalls of ignoring topography in snow retrievals: a case study with EMIT, Available at SSRN 4707319, 2024.

Bonilla, E., Mickley, L., Beaudon, E., Thompson, L., Rodriguez, W., Encarnación, R. C., Whicker, C., Flanner, M., Schmitt, C., and Ginot, P.: Contribution of biomass burning to black carbon deposition on Andean glaciers: consequences for radiative forcing, Environmental Research Letters, 18, 024 031, 2023.

Brock, B. W., Willis, I. C., and Sharp, M. J.: Measurement and parameterization of albedo variations at Haut Glacier d'Arolla, Switzerland, Journal of Glaciology, 46, 675–688, 2000.

Brock, B. W., Willis, I. C., and Sharp, M. J.: Measurement and parameterization of aerodynamic roughness length variations at Haut Glacier d'Arolla, Switzerland, Journal of Glaciology, 52, 281–297, 2006.

Cogley, J.: others (2011) Glossary of glacier mass balance and related terms, 2011.

Collier, E., Mölg, T., Maussion, F., Scherer, D., Mayer, C., and Bush, A.: High-resolution interactive modelling of the mountain glacier–atmosphere interface: an application over the Karakoram, The Cryosphere, 7, 779–795, 2013.

Cook, J. M., Hodson, A. J., and Irvine-Fynn, T. D.: Supraglacial weathering crust dynamics inferred from cryoconite hole hydrology, Hydrological Processes, 30, 433–446, 2016.

Cremona, A., Huss, M., Landmann, J. M., Borner, J., and Farinotti, D.: European heat waves 2022: contribution to extreme glacier melt in Switzerland inferred from automated ablation readings, The Cryosphere, 17, 1895–1912, 2023.

Dadic, R., Mullen, P. C., Schneebeli, M., Brandt, R. E., and Warren, S. G.: Effects of bubbles, cracks, and volcanic tephra on the spectral albedo of bare ice near the Transantarctic Mountains: Implications for sea glaciers on Snowball Earth, Journal of Geophysical Research: Earth Surface, 118, 1658–1676, 2013.

Di Mauro, B.: A darker cryosphere in a warming world, Nature Climate Change, 10, 979–980, 2020.

Di Mauro, B. and Fugazza, D.: Pan-Alpine glacier phenology reveals lowering albedo and increase in ablation season length, Remote Sensing of Environment, 279, 113 119, 2022.

Di Mauro, B., Baccolo, G., Garzonio, R., Giardino, C., Massabò, D., Piazzalunga, A., Rossini, M., and Colombo, R.: Impact of impurities and cryoconite on the optical properties of the Morteratsch Glacier (Swiss Alps), The Cryosphere, 11, 2393–2409, 2017.

Di Mauro, B., Garzonio, R., Baccolo, G., Franzetti, A., Pittino, F., Leoni, B., Remias, D., Colombo, R., and Rossini, M.: Glacier algae foster ice-albedo feedback in the European Alps, Scientific Reports, 10, 4739, 2020.

Di Mauro, B., Cogliati, S., Bohn, N., Traversa, G., Garzonio, R., Tagliabue, G., Bramati, G., Cremonese, E., Julitta, T., Guanter, L., et al.: Evaluation of PRISMA products over snow in the Alps and Antarctica, Earth and Space Science, 11, e2023EA003 482, 2024.

Draeger, C., Radić, V., White, R. H., and Tessema, M. A.: Evaluation of reanalysis data and dynamical downscaling for surface energy
540   balance modeling at mountain glaciers in western Canada, The Cryosphere, 18, 17–42, 2024.

Drusch, M., Del Bello, U., Carlier, S., Colin, O., Fernandez, V., Gascon, F., Hoersch, B., Isola, C., Laberinti, P., Martimort, P., Meygret, A., Spoto, F., Sy, O., Marchese, F., and Bargellini, P.: Sentinel-2: ESA's optical high-resolution mission for GMES operational services, Remote sensing of Environment, 120, 25–36, 2012.

Dumont, M., Gardelle, J., Sirguey, P., Guillot, A., Six, D., Rabatel, A., and Arnaud, Y.: Linking glacier annual mass balance and glacier
545   albedo retrieved from MODIS data, The Cryosphere, 6, 1527–1539, 2012.

Eidhammer, T., Booth, A., Decker, S., Li, L., Barlage, M., Gochis, D., Rasmussen, R., Melvold, K., Nesje, A., and Sobolowski, S.: Mass balance and hydrological modeling of the Hardangerjøkulen ice cap in south-central Norway, Hydrology and Earth System Sciences, 25, 4275–4297, 2021.

Fischer, A., Stocker-Waldhuber, M., Frey, M., and Bohleber, P.: Contemporary mass balance on a cold Eastern Alpine ice cap as a potential
550   link to the Holocene climate, Scientific Reports, 12, 1331, 2022.

Fugazza, D., Senese, A., Azzoni, R. S., Maugeri, M., and Diolaiuti, G. A.: Spatial distribution of surface albedo at the Forni Glacier (Stelvio National Park, Central Italian Alps), Cold Regions Science and Technology, 125, 128–137, 2016.

Fugazza, D., Senese, A., Azzoni, R. S., Maugeri, M., Maragno, D., and Diolaiuti, G. A.: New evidence of glacier darkening in the Ortles-Cevedale group from Landsat observations, Global and Planetary Change, 178, 35–45, 2019.

555   Garzonio, R., Di Mauro, B., Cogliati, S., Rossini, M., Panigada, C., Delmonte, B., Maggi, V., and Colombo, R.: A novel hyperspectral system for high resolution imaging of ice cores: Application to light-absorbing impurities and ice structure, Cold Regions Science and Technology, 155, 47–57, 2018.

Geibel, L., Huss, M., Kurzböck, C., Hodel, E., Bauder, A., and Farinotti, D.: Rescue and homogenisation of 140 years of glacier mass balance data in Switzerland, Earth System Science Data Discussions, 2022, 1–30, 2022.

560   Gilardoni, S., Di Mauro, B., and Bonasoni, P.: Black carbon, organic carbon, and mineral dust in South American tropical glaciers: A review, Global and Planetary Change, 213, 103 837, 2022.

Goelles, T. and Bøggild, C. E.: Albedo reduction of ice caused by dust and black carbon accumulation: a model applied to the K-transect, West Greenland, Journal of Glaciology, 63, 1063–1076, 2017.

Gorelick, N., Hancher, M., Dixon, M., Ilyushchenko, S., Thau, D., and Moore, R.: Google Earth Engine: Planetary-scale geospatial analysis
565   for everyone, Remote sensing of Environment, 202, 18–27, 2017.

Gunnarsson, A., Gardarsson, S. M., Pálsson, F., Jóhannesson, T., and Sveinsson, Ó. G.: Annual and inter-annual variability and trends of albedo of Icelandic glaciers, The Cryosphere, 15, 547–570, 2021.

Gunnarsson, A., Gardarsson, S. M., and Pálsson, F.: Modeling of surface energy balance for Icelandic glaciers using remote-sensing albedo, The Cryosphere, 17, 3955–3986, 2023.

570   Hartl, L., Felbauer, L., Schwaizer, G., and Fischer, A.: Small-scale spatial variability in bare-ice reflectance at Jamtalferner, Austria, The Cryosphere, 14, 4063–4081, 2020.

Hartl, L., Schmitt, P., Schuster, L., Helfricht, K., Abermann, J., and Maussion, F.: Recent observations and glacier modeling point towards near complete glacier loss in western Austria (Ötztal and Stubai mountain range) if 1.5° C is not met, EGUsphere, 2024, 1–33, 2024a.

Hartl, L., Seiser, B., Stocker-Waldhuber, M., Baldo, A., Lauria, M. V., and Fischer, A.: Glaciological and meteorological monitoring at Long Term Ecological Research (LTER) sites Mullwitzkees and Venedigerkees, Austria, 2006–2022, Earth System Science Data, 16, 4077–4101, 2024b.

Helfricht, K., Hartl, L., Stocker-Waldhuber, M., Seiser, B., and Fischer, A.: Glacier inventory Ötztal Alps 2017 [dataset], https://doi.pangaea.de/10.1594/PANGAEA.965798, 2024.

Hugonnet, R., McNabb, R., Berthier, E., Menounos, B., Nuth, C., Girod, L., Farinotti, D., Huss, M., Dussaillant, I., Brun, F., et al.: Accelerated global glacier mass loss in the early twenty-first century, Nature, 592, 726–731, 2021.

Hukseflux: USER MANUAL NR01 / RA01, Hukseflux Thermal Sensors, https://www.hukseflux.com/uploads/product-documents/NR01_RA01_manual_v2303.pdf, 2023.

Immerzeel, W. W., Pellicciotti, F., and Shrestha, A. B.: Glaciers as a proxy to quantify the spatial distribution of precipitation in the Hunza basin, Mountain research and development, 32, 30–38, 2012.

Irvine-Fynn, T. D., Sanz-Ablanedo, E., Rutter, N., Smith, M. W., and Chandler, J. H.: Measuring glacier surface roughness using plot-scale, close-range digital photogrammetry, Journal of Glaciology, 60, 957–969, 2014.

Jakob, L. and Gourmelen, N.: Glacier mass loss between 2010 and 2020 dominated by atmospheric forcing, Geophysical Research Letters, 50, e2023GL102 954, 2023.

Klok, E. L. and Oerlemans, J.: Model study of the spatial distribution of the energy and mass balance of Morteratschgletscher, Switzerland, Journal of Glaciology, 48, 505–518, 2002.

Liang, S.: Narrowband to broadband conversions of land surface albedo I: Algorithms, Remote sensing of environment, 76, 213–238, 2001.

Marshall, S. J.: Regime shifts in glacier and ice sheet response to climate change: examples from the Northern Hemisphere, Frontiers in Climate, 3, 702 585, 2021.

Miles, E., McCarthy, M., Dehecq, A., Kneib, M., Fugger, S., and Pellicciotti, F.: Health and sustainability of glaciers in High Mountain Asia, Nature Communications, 12, 2868, 2021.

Naegeli, K. and Huss, M.: Sensitivity of mountain glacier mass balance to changes in bare-ice albedo, Annals of Glaciology, 58, 119–129, 2017.

Naegeli, K., Damm, A., Huss, M., Schaepman, M., and Hoelzle, M.: Imaging spectroscopy to assess the composition of ice surface materials and their impact on glacier mass balance, Remote Sensing of Environment, 168, 388–402, 2015.

Naegeli, K., Damm, A., Huss, M., Wulf, H., Schaepman, M., and Hoelzle, M.: Cross-comparison of albedo products for glacier surfaces derived from airborne and satellite (Sentinel-2 and Landsat 8) optical data, Remote Sensing, 9, 110, 2017.

Naegeli, K., Huss, M., and Hoelzle, M.: Change detection of bare-ice albedo in the Swiss Alps, The Cryosphere, 13, 397–412, 2019.

Oerlemans, J., Giesen, R., and Van den Broeke, M.: Retreating alpine glaciers: increased melt rates due to accumulation of dust (Vadret da Morteratsch, Switzerland), Journal of Glaciology, 55, 729–736, 2009.

Pandžic, M., Mihajlovic, D., Pandžic, J., and Pfeifer, N.: Assessment of the geometric quality of sentinel-2 data, The International Archives of the Photogrammetry, Remote Sensing and Spatial Information Sciences, 41, 489–494, 2016.

Pasquarella, V. J., Brown, C. F., Czerwinski, W., and Rucklidge, W. J.: Comprehensive quality assessment of optical satellite imagery using weakly supervised video learning, in: Proceedings of the IEEE/CVF Conference on Computer Vision and Pattern Recognition, pp. 2124–2134, 2023.

Paul, F., Machguth, H., and Kääb, A.: On the impact of glacier albedo under conditions of extreme glacier melt: the summer of 2003 in the Alps, EARSeL eProceedings, 4, 139–149, 2005.

Paul, F., Winsvold, S. H., Kääb, A., Nagler, T., and Schwaizer, G.: Glacier remote sensing using Sentinel-2. Part II: Mapping glacier extents and surface facies, and comparison to Landsat 8, Remote Sensing, 8, 575, 2016.

Pelto, M.: Forecasting temperate alpine glacier survival from accumulation zone observations, The Cryosphere, 4, 67–75, 2010.

615 Pelto, M. S.: Methods for assessing and forecasting the survival of North Cascade, Washington glaciers, Quaternary International, 235, 70–76, 2011.

Picard, G., Dumont, M., Lamare, M., Tuzet, F., Larue, F., Pirazzini, R., and Arnaud, L.: Spectral albedo measurements over snow-covered slopes: theory and slope effect corrections, The Cryosphere, 14, 1497–1517, 2020.

Ren, S., Miles, E. S., Jia, L., Menenti, M., Kneib, M., Buri, P., McCarthy, M. J., Shaw, T. E., Yang, W., and Pellicciotti, F.: Anisotropy
620 parameterization development and evaluation for glacier surface albedo retrieval from satellite observations, Remote Sensing, 13, 1714, 2021.

Rossini, M., Garzonio, R., Panigada, C., Tagliabue, G., Bramati, G., Vezzoli, G., Cogliati, S., Colombo, R., and Di Mauro, B.: Mapping surface features of an alpine glacier through multispectral and thermal drone surveys, Remote Sensing, 15, 3429, 2023.

Rounce, D. R., Hock, R., Maussion, F., Hugonnet, R., Kochtitzky, W., Huss, M., Berthier, E., Brinkerhoff, D., Compagno, L., Copland, L.,
625 et al.: Global glacier change in the 21st century: Every increase in temperature matters, Science, 379, 78–83, 2023.

Sauter, T., Arndt, A., and Schneider, C.: COSIPY v1. 3–an open-source coupled snowpack and ice surface energy and mass balance model, Geoscientific Model Development, 13, 5645–5662, 2020.

Schaepman-Strub, G., Schaepman, M. E., Painter, T. H., Dangel, S., and Martonchik, J. V.: Reflectance quantities in optical remote sensing—Definitions and case studies, Remote sensing of environment, 103, 27–42, 2006.

630 Schuster, L., Rounce, D. R., and Maussion, F.: Glacier projections sensitivity to temperature-index model choices and calibration strategies, Annals of Glaciology, pp. 1–16, 2023.

Shaw, T. E., Ulloa, G., Farías-Barahona, D., Fernandez, R., Lattus, J. M., and McPhee, J.: Glacier albedo reduction and drought effects in the extratropical Andes, 1986–2020, Journal of Glaciology, 67, 158–169, 2021.

Spagnesi, A., Bohleber, P., Barbaro, E., Feltracco, M., De Blasi, F., Dreossi, G., Stocker-Waldhuber, M., Festi, D., Gabrieli, J., Gambaro, A.,
635 et al.: Preservation of chemical and isotopic signatures within the Weißseespitze millennial old ice cap (Eastern Alps), despite the ongoing ice loss, Frontiers in Earth Science, 11, 1322 411, 2023.

Stocker-Waldhuber, M., Seiser, B., and Fischer, A.: Meteorological data Weißseespitze/Austria, 2017 et seq, https://doi.org/10.1594/PANGAEA.939830, 2022a.

Stocker-Waldhuber, M., Seiser, B., and Fischer, A.: Ice thickness data Weißseespitze/Austria, https://doi.org/10.1594/PANGAEA.939817,
640 2022b.

Takeuchi, N., Kohshima, S., and Seko, K.: Structure, formation, and darkening process of albedo-reducing material (cryoconite) on a Himalayan glacier: a granular algal mat growing on the glacier, Arctic, Antarctic, and Alpine Research, 33, 115–122, 2001.

Tedstone, A. J., Cook, J. M., Williamson, C. J., Hofer, S., McCutcheon, J., Irvine-Fynn, T., Gribbin, T., and Tranter, M.: Algal growth and weathering crust state drive variability in western Greenland Ice Sheet ice albedo, The Cryosphere, 14, 521–538, 2020.

645 Traversa, G. and Di Mauro, B.: Weathering crust formation outpaces melt-albedo feedback on blue ice shelves of East Antarctica, Communications Earth & Environment, 5, 740, 2024.

Traversa, G., Fugazza, D., Senese, A., and Frezzotti, M.: Landsat 8 OLI broadband albedo validation in Antarctica and Greenland, Remote Sensing, 13, 799, 2021.

Volery, A., Naegeli, K., and Barandun, M.: The sub-seasonal and interannual spatio-temporal variability of bare-ice albedo of Abramov
Glacier, Kyrgyzstan, Journal of Glaciology, pp. 1–31, 2025.

Voordendag, A., Prinz, R., Schuster, L., and Kaser, G.: Brief communication: The Glacier Loss Day as an indicator of a record-breaking
negative glacier mass balance in 2022, The Cryosphere, 17, 3661–3665, 2023.

Weiser, U., Olefs, M., Schöner, W., Weyss, G., and Hynek, B.: Correction of broadband snow albedo measurements affected by unknown
slope and sensor tilts, The Cryosphere, 10, 775–790, 2016.

Williamson, S. N. and Menounos, B.: The influence of forest fire aerosol and air temperature on glacier albedo, western North America,
Remote Sensing of Environment, 267, 112 732, 2021.

Zekollari, H., Huss, M., and Farinotti, D.: Modelling the future evolution of glaciers in the European Alps under the EURO-CORDEX RCM
ensemble, The Cryosphere, 13, 1125–1146, 2019.

Zhang, Y., Kang, S., Sprenger, M., Cong, Z., Gao, T., Li, C., Tao, S., Li, X., Zhong, X., Xu, M., et al.: Black carbon and mineral dust in snow
cover on the Tibetan Plateau, The Cryosphere, 12, 413–431, 2018.

Zhang, Y., Gao, T., Kang, S., Shangguan, D., and Luo, X.: Albedo reduction as an important driver for glacier melting in Tibetan Plateau and
its surrounding areas, Earth-Science Reviews, 220, 103 735, 2021.